Mechanisms driving glacial deep ocean deoxygenation

Ellen Cliff

University College

University of Oxford

A thesis submitted for the degree of

Masters of Science by Research

6 October 2022

Acknowledgements

This thesis was written in Oxford, England and on the unceded lands of the Ngunnawal people.

Thank you first to my supervisors Samar Khatiwala, Gideon Henderson, Andreas Schmittner for your guidance throughout this process. And thank you especially for all the homemade food, Samar!

I could not have undertaken this 'journey' without the support, moral and financial, of the Rhodes Trust, especially Mary Eaton and Elizabeth Kiss. And thank you to keeping me keel mostly even, Brigid, Audrey and Tracey.

Thank you to my not-so-new Oxford friends, old Aussie friends and my family that saw me through this challenging process: Sophie, Gwen and Ricky, Lauren, Ella, Maddie, Steve and Louise, Jeremy (and Tink), Nan, Mum and Dad. I couldn't have crawled across the finish line without you. I love you all.

Abstract

Deep ocean deoxygenation inferred from proxies has been used to support the hypothesis that lower atmospheric carbon dioxide during glacial times was due to an increase in the strength of the ocean's biological pump. This relies on the assumption that surface ocean oxygen (O_2) is equilibrated with the atmosphere such that any O_2 deficiency observed in deep waters is a result of organic matter respiration consuming O_2 and producing dissolved inorganic carbon. However, this assumption has been shown to be imperfect because of disequilibrium. Here I use an Earth System Model tuned to a suite of observations, which reproduces the pattern of glacial-to-Holocene oxygenation change seen in proxy data, to show that disequilibrium plays an important role in glacial deep ocean deoxygenation. Using a novel decomposition method to track O_2, I find a whole-ocean loss of 33 Pmol O_2 from the preindustrial to the Last Glacial Maximum (LGM) despite a 27 Pmol gain from increased solubility due to cooler temperatures. This loss is driven by biologically-mediated O_2 disequilibrium, which increases from contributing 10% of the reduction of the O_2 inventory from solubility equilibrium in the preindustrial, to 27% during the LGM. Sea ice and iron fertilization are found to be the largest contributors to LGM deoxygenation, which occurs despite overall reduced production and respiration of organic matter in the glacial ocean. These results challenge the notion that deep ocean glacial deoxygenation was caused by a stronger biological pump or more sluggish circulation, and instead highlights the importance and previously under-appreciated role of O_2 disequilibrium.

Contents

List of Figures

List of Tables

List of Abbreviations

AABW . . . . Antarctic Bottom Water

AMOC . . . . Atlantic Meridional Overturning Circulation

AOU . . . . . Apparent Oxygen Utilisation

Au-U . . . . . Authigenic Uranium

CMIP . . . . . Coupled Model Intercomparison Project

DIC . . . . . Dissolved Inorganic Carbon

DOC . . . . . Dissolved Organic Carbon

ESCM . . . . . Earth System Climate Model

GCM . . . . . General Circulation Model

GtC . . . . . Gigatonnes of Carbon

LGM . . . . . Last Glacial Maximum

MOBI2.0 . . . Model of Ocean Biogeochemistry and Isotopes version 2.0

pCO_2 . . . . . Partial Pressure of Atmospheric CO_2

PIC . . . . . Particulate Inorganic Carbon

PMIP . . . . . Paleoclimate Modelling Intercomparison Project

ppm . . . . . Parts Per Million by Volume

SOCCOM . . Southern Ocean Carbon and Climate Observations and Modelling project

SST . . . . . Sea Surface Temperature

TOU . . . . . True Oxygen Utilisation

UVic . . . . . University of Victoria Earth System Model

Chapter 1

Introduction

Contents

1.1 The ocean carbon cycle

The ocean is the second largest reservoir of carbon in the global carbon cycle, after the lithosphere. In preindustrial times, the ocean is estimated to have contained a total of ∼40,450 Gt of carbon (GtC) while the terrestrial biosphere, which includes permafrost and soil, contained 3350 GtC and the atmosphere 591 GtC [1]. This makes the ocean an incredibly important part of the carbon cycle and global climate.

The ocean can store a large amount of dissolved carbon dioxide (CO_2) due to the high buffering capacity of seawater. When CO_2 from the atmosphere dissolves in seawater, a fraction of the dissolved gas reacts with water to form carbonic acid (H_2CO_3) which dissociates further into bicarbonate (HCO_3^-) and carbonate ions (CO_3^{2-}) (Fig. 1.1) [2]. These contribute to dissolved inorganic carbon (DIC), which is the sum of dissolved CO_2, bicarbonate (HCO_3^-) and carbonate (CO_3^{2-}) ions in seawater. Under typical seawater conditions at pH ∼8.1 the majority of this is the bicarbonate ion [2], which is the major carbon source utilised by phytoplankton during photosynthesis. The organic carbon produced then cycles through the

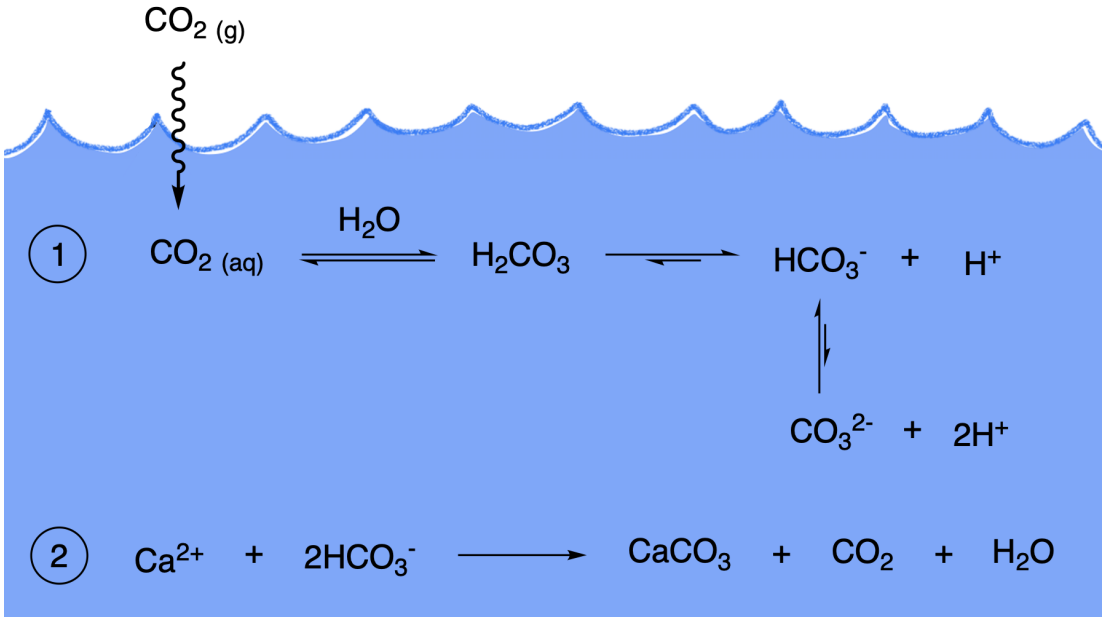

Figure 1.1: Equation set 1 shows the transfer of CO_2 from the atmosphere into seawater and subsequent reaction with water to form carbonic acid (H_2CO_3) and dissociation into bicarbonate (HCO_3^-) and carbonate (CO_3^{2-}) ions. Equation set 2 shows the reaction of Ca^{2+} ions with bicarbonate to produce calcium carbonate ($CaCO_3^{2-}$), CO_2 and water.

food chain (Fig. 1.2). Phytoplankton are consumed by heterotrophs who use this fixed carbon, and the eventual consumption of phytoplankton and heterotrophs by bacteria consumes O_2 and releases DIC back into the water column. The export of organic matter from the surface ocean (top ~100 m) to the intermediate and deep ocean results in an accumulation of DIC and a depletion of O_2 down the water column, as these waters are not in contact with the atmosphere. This process of transfer of carbon from the surface to deep ocean is called the "soft-tissue pump".

Although, at any one time, marine biota are only a minor component of the total oceanic carbon reservoir (3 GtC), over century to millennial timescales, the soft-tissue pump enables the accumulation of large amounts of carbon in the form of dissolved organic carbon (700 GtC) and organic matter buried in seafloor sediments (1,750 GtC). In combination with the solubility pump, which is the transfer of carbon between the atmosphere and the surface ocean that occurs through the physical process of temperature-driven solubility (Fig. 1.2), this results in high accumulation of DIC in the surface ocean (900 GtC) and the intermediate and

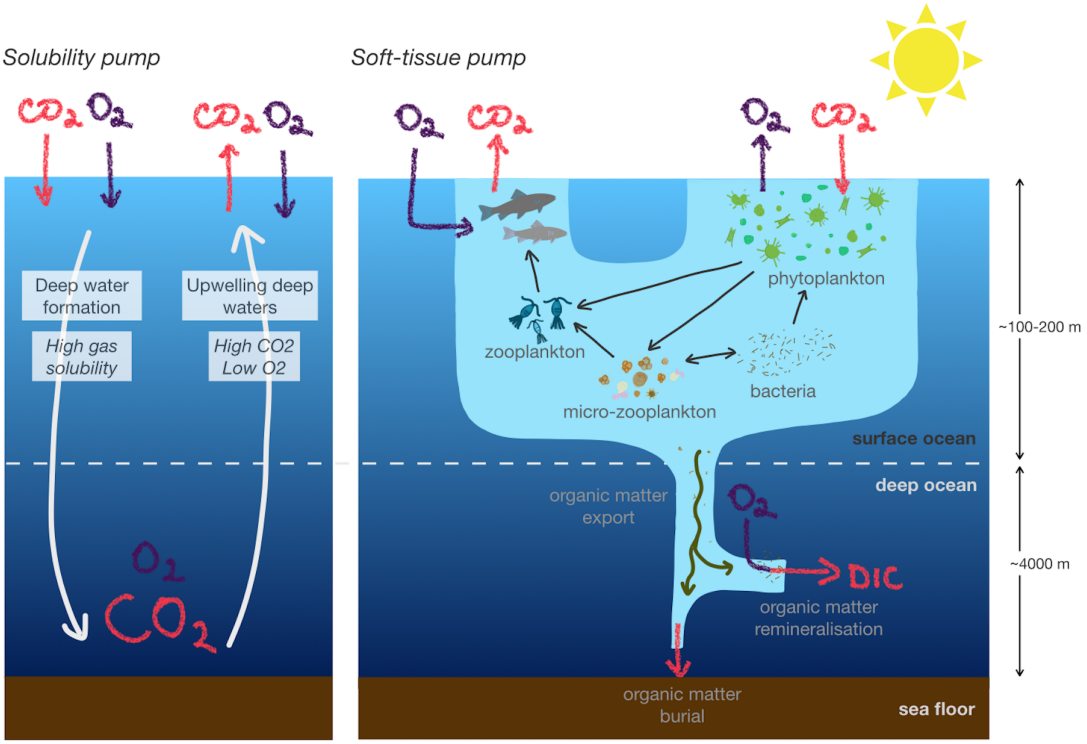

Figure 1.2: The physical (left) and soft-tissue (right) pumps of the carbon and O_2 systems. In the physical pump both CO_2 and O_2 are absorbed by cold waters at the site of deep water formation. At the site of upwelling deep waters, carbon-rich and oxygen-poor waters come to the surface such that CO_2 will be transferred from the surface waters to the atmosphere, while O_2 will instead be transferred from the atmosphere to the ocean to re-equilibrate the waters. The soft-tissue pump is shown with the transfer of CO_2 that is sequestered by phytoplankton which then produce O_2 in the surface ocean. Phytoplankton enter the food chain where heterotrophs consume O_2 and excrete carbon, and eventual aerobic respiration by bacteria further consumes dissolved O_2 and releases DIC into the water column. The small amount of refractory organic matter that is not consumed in the water column is buried in ocean sediments.

deep ocean (37,100 GtC) [1]. In regions of deep water formation, such as the North Atlantic and Southern Ocean, waters are cold and dense meaning both CO_2 and O_2 solubility is high, assisting in the transfer of these species to the deep ocean [3]. The soft-tissue pump intensifies transfer of carbon to the deep ocean through export of organic matter and remineralisation of organic matter at depth to produce dissolved inorganic carbon (DIC). Conversely, biologically-produced calcium carbonate removes alkalinity and produces CO_2 in the surface ocean, and dissolution in the deep replaces alkalinity and consumes CO_2 (carbonate pump) (Fig. 1.1). The soft-tissue, solubility and carbonate pumps all play important

roles over millennial timescales.

While carbon in the surface ocean can be exchanged with atmospheric CO_2 on a timescale of weeks, DIC is sequestered in the intermediate and deep ocean for decades to millennia. Because the atmosphere has a comparably small carbon inventory, a relatively small shift in the amount of carbon stored in the ocean can have profound effects on atmospheric CO_2 and planetary climate.

1.2 O_2 and CO_2 in the Ocean

The buffering capacity of seawater causes slower equilibration of dissolved CO_2 with the atmosphere (∼1 year) than gases such as O_2 that equilibrate relatively quickly (∼weeks). As a result, the majority of pre-industrial CO_2 is stored in the ocean (98.5%) rather than the atmosphere (1.5%), whereas, due to its poorer solubility, very little O_2 is stored in the ocean (0.6%) compared to the atmosphere (99.4%) [4]. O_2 is inversely connected to carbon through the soft-tissue pump; the formation of organic matter by phytoplankton uses dissolved carbon, nitrate and phosphate from seawater, and releases O_2. When organic matter is remineralised by aerobic respiration dissolved O_2 is consumed, and carbon, nitrate and phosphate are returned to the water column (Fig. 1.2). The standard fixed Redfield stoichiometry between these major nutrients in phytoplankton and O_2 is estimated to be C:N:P:-O_2 = 1:16(±1):117(±14):170(±10) [5]. Variability in stoichiometry will have an effect both on the transfer of carbon to the deep ocean via the soft-tissue pump, and the degree to which O_2 is produced in the surface and consumed at depth. Unlike the soft-tissue pump, the solubility pump acts similarly for both carbon and O_2 at high latitudes. In high latitude waters where deep water forms, cold waters have higher solubility for both gases, leading to an influx of both CO_2 and O_2 (Fig. 1.2). When deep waters are upwelled (ventilated), however, these carbon-rich waters will outgas CO_2 to the atmosphere to equilibrate, while O_2 ingassing will occur to restore equilibrium of these O_2-depleted waters.

1.3 Preformed tracers and air-sea gas disequilibrium

In ocean biogeochemical models, preformed tracers are the quantities of a particular chemical set at the surface of the ocean that are conservatively and passively circulated through the model. The preformed concentrations of both O_2 and CO_2 are affected by air-sea gas exchange, while nutrients such as phosphate, are not. Because O_2 has a more rapid equilibration timescale than CO_2 it has often been considered to be at, or near, equilibrium (*eg* [6, 7]). Biological processes at the surface affect these preformed quantities, as do the properties of upwelled deep waters that these surface waters are mixed with. Surface water O_2 and CO_2 can be disequilibreated with the atmosphere, and an ingassing or outgassing will occur over time to re-equilibrate the waters while they are at the surface and in contact with the atmosphere. If these waters do not reach equilibrium before they circulate into the interior of the ocean, this preformed disequilibrium will be carried into intermediate and deep waters. For O_2, the disequilibrium component of preformed O_2 can be calculated by taking the difference between the observed preformed O_2 tracer concentration and the tracer for theoretical preformed concentration for waters at equilibrium.

1.4 The Last Glacial Maximum

The Last Glacial Maximum (LGM) was the period 22,000 to 19,000 years before present when ice age conditions were at their peak. Glacial-interglacial cycles of the past two million years were driven by orbital changes (eccentricity, obliquity, and precession), however, changes in temperature were tightly coupled with variations in atmospheric CO_2 that enhance the magnitude of warming and cooling. During the LGM, atmospheric CO_2 was $\sim$90 ppm lower than pre-industrial levels which reduced global temperatures further than the effect of orbital changes alone. This relationship is very tightly linked (Fig. 1.3).

Lower atmospheric CO_2 in the LGM is largely attributed to enhanced carbon storage in the deep ocean [9]. Different mechanisms have been proposed to explain

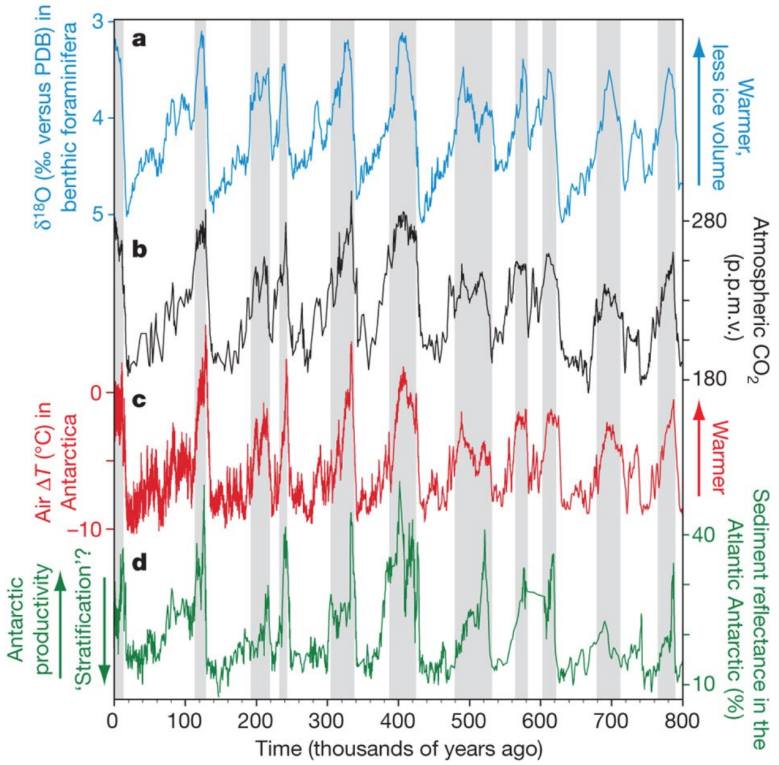

Figure 1.3: Southern hemisphere records of changing temperature, sea ice volume, productivity and, atmospheric CO_2 over 800,000 years compiled by Sigman et al. [8].

this drawdown. The mechanisms that have emerged as the most important for increasing glacial ocean carbon storage include larger sea ice extent [10, 11], iron fertilisation, particularly of the high nutrient Southern Ocean region [12, 13], a strengthened biological pump due to higher concentrations of macronutrients resulting from lower sea levels [9, 13], more sluggish circulation preventing ventilation of the deep ocean [8, 14, 15], and lower global temperatures enhancing CO_2 solubility [4, 16–19]. The importance of these processes in changing carbon storage over glacial-interglacial cycles is still the subject of intense scientific debate. A further process affecting ocean carbon storage in the LGM is the role of air-sea gas disequilibrium of CO_2, and, unlike the aforementioned processes, this has only recently been explicitly introduced into the debate [20].

A number of recent studies have invoked increased strength of the biological soft-tissue pump to explain increased glacial ocean carbon storage [15, 21, 22]. These studies use Apparent Oxygen Utilisation (AOU) to estimate respired carbon,

or increases in epibenthic foraminiferal $\delta^{13}C$ during the LGM, as evidence for changes in the strength of the biological pump. AOU is the most widely used observational method available to oceanographers for estimating the amount of remineralised carbon stored in the deep ocean. AOU is calculated by taking the difference in the theoretical quantity of fully saturated O_2 in a parcel of water ($O_{2,sat}$): calculated from potential temperature (θ) and salinity(S)) of the measured O_2 value in that water parcel. Any deficit of utilised O_2 is assumed to be the result of respiration of organic matter [23] and so is used to estimate respired carbon in the deep ocean. AOU is often calculated in model simulations as only temperature, salinity and O_2 need to be known, saving computational resources needed to track preformed tracer concentrations. This can be then used to calculate respired carbon in ocean biogeochemical models. A handful of studies have addressed the problem of assuming O_2 equilibration and using AOU to trace O_2 consumption in the modern ocean [24–27], however, a rigorous study of the mechanisms affecting O_2 disequilibrium and the role of disequilibrium in glacial conditions has not been conducted. Despite this, O_2 proxy data is often used to explain changes in deep ocean carbon storage [7, 13, 21].

Modelling O_2 disequilibrium in the preindustrial and LGM is the basis of the research in this thesis. The aim is to understand the relationship between O_2 disequilibrium, carbon disequilibrium and carbon storage estimates. The accurate method of decomposing carbon systems in seawater described in [20] was applied to the O_2 system to quantify and better understand the distribution of O_2 in the preindustrial and glacial oceans.

Chapter 2

Literature Review

Contents

One of the major goals and motivations of paleoclimate studies in the last 40 years has been to identify the combination of processes that led to a drop in atmospheric CO_2 seen during glacial events, and the rise in CO_2 during deglaciation events. The rise and fall of atmospheric CO_2 has been shown to be temporally correlated with orbitally driven glacial-interglacial cycles, exacerbating temperature variability during these cycles. During the Last Glacial Maximum (LGM) the global temperature was 2.5°C cooler than the preindustrial era, and atmospheric CO_2 was ∼90 ppm lower than the preindustrial level [8]. Being in the geologically recent past, a broad array of global ocean and land-based geochemical data for the LGM have been developed and accrued for several decades. This has allowed geochemists and modellers to develop hypotheses about why global CO_2 dropped during this period, and to better understand and model the drivers of oceanic CO_2 storage under different climate states including high CO_2 futures. The contribution of different biological and physical processes in the global ocean to the distribution of oceanic O_2 concentrations, and how these interact with the distribution of carbon

is the focus of this work. The research underpinning and motivating this work is the focus of this literature review.

2.1 Ocean CO_2 levels in the LGM

In 1977, the book "The Fate of Fossil Fuel CO_2 in the Oceans" was published, bringing together the then-current science on atmospheric CO_2 levels, the earth's past, present and future climate, and the oceans [28]. This work incorporated the current findings and hypotheses surrounding the Last Glacial Maximum (LGM) and N. Shackleton included a chapter that showed the glacial deep ocean ratio of $^{13}C/^{12}C$ was lower than during the interglacial period [29]. Shackleton hypothesised that this was due to a reduced forest-soil organic carbon reservoir during glacial times. The implication of this was that because there was a smaller terrestrial biosphere, there must have been higher atmospheric CO_2 content during the LGM. Just three years later, two groups independently reported measurements of atmospheric gases trapped in ice cores from the LGM [30, 31]. These groups both showed that glacial atmospheric CO_2 was significantly lower in the LGM than in the Holocene. This called for a new hypothesis to reconcile these results.

Broecker (1982) provided a first hypothesis that explained the ice core data and geochemical data from surface and deep-sea sediments [9]. Broecker proposed that the reduction in atmospheric CO_2 was largely due to carbon (in the form of organic matter) and phosphorus being transferred from the surface ocean to another reservoir in approximately Redfield proportions. He proposed using deep ocean dissolved O_2 as a possible cross-check for changes in phosphate distribution which could later be estimated using cadmium/calcium levels in benthic and planktonic foraminifera [32, 33], and therefore changes in organic carbon storage. This hypothesis highlighted that changes in ocean chemistry could drive large changes in atmospheric CO_2 content over glacial cycles with the total DIC content of the oceans increasing during glacial times, reducing atmospheric CO_2.

The mechanisms for this enhanced carbon storage were largely attributed to changes in the biologically-mediated transfer of particulate organic carbon from

the surface ocean to the deep ocean, via the soft-tissue pump [16]. The increase in deep ocean carbon storage was hypothesised to be caused by an increase in the efficiency of the soft-tissue pump as there was less phosphate being removed through burial on continental shelves as the glacial ocean had lower sea levels [9, 34]. In about two thirds of the modern ocean, nitrate is the limiting nutrient, however, for nitrogen-fixing diazotrophs, phosphorus is the limiting nutrient [35]. In the LGM, higher concentrations of preformed phosphate could be utilised by phosphorus-limited diazotrophs increasing the drawdown of carbon, a hypothesis demonstrating that nutrient-driven ecosystem composition changes could alter the global carbon cycle [36].

In high nutrient-low chlorophyll (HNLC) zones, nitrate, phosphate and silicate are abundant while iron is the limiting nutrient. The Southern Ocean is an extremely important HNLC region due to differences in bioavailable iron concentrations between the preindustrial and LGM oceans. The iron hypothesis was put forward by Martin [12] in 1990, and provided a crucial piece of the puzzle required to understand changes in ocean carbon storage over glacial-interglacial periods. In the glacial period, there were stronger winds and a dustier atmosphere [37] resulting in more continental dust, containing bioavailable iron, being deposited over the oceans, particularly the iron-poor Southern Ocean [38]. This increased the export of carbon and nutrients from the surface of high latitude waters to the deep ocean, accounting for a drop in atmospheric CO_2. Iron flux reconstructions from sediments have since confirmed the importance of iron fertilisation over the Southern Ocean [38]. The effect of glacial changes in dust deposition and bioavailable iron concentrations to the stoichiometry of dissolved inorganic carbon (DIC) utilisation and O_2 production by different phytoplankton remains challenging to model accurately. Some of these difficulties stem from the complexity of ecosystem responses [21] and the effect of iron ligand chemistry under different redox conditions driven by changes to O_2 concentrations [39]. As such, making accurate models of the iron cycle is a continuing challenge [40]. The early hypotheses of nutrient-driven changes to the efficiency of the biological soft-tissue pump did not take into account the more indirect effects

of biology on the storage of carbon that appear when combined with physical effects such as circulation and air-sea gas exchange, which, for instance, control the amount of biological carbon that returns to the deep ocean via subduction following circulation-driven upwelling and carbon outgassing. These interactions become important in later efforts to model and understand LGM ocean carbon cycling [41].

Other early hypotheses of LGM deep ocean carbon storage involved the role of increased global ocean alkalinity through changes to the "carbonate pump". This was proposed through multiple mechanisms including the dissolution of coral reefs [42] and through changes in the interaction between carbonate and sediments [43] including changes in calcite lysocline depth [44]. As the uptake of CO_2 into the ocean increased, carbonate chemistry shifts such that the carbonate lysocline shoals [44]. The result is the dissolution of carbonate sediments to shallower depths, increasing global ocean alkalinity, which in turn increases the buffering capacity of the global ocean, helping to further drawdown CO_2 from the atmosphere [8].

Coarse resolution box models have been developed to test these and other hypotheses. Toggweiler [45] showed with their model that low LGM CO_2 could be explained by a reduction in the ventilation of deep-water formed at high latitudes. Alternatively, Stephens and Keeling [10] used a box model to demonstrate that sea ice could account for approximately two thirds of the LGM atmospheric CO_2 drop through the reduction of air-sea gas exchange in the Southern Ocean around Antarctica. Air-sea gas exchange of CO_2 is slowed by the buffering capacity of sea water. This is not the case for O_2 which equilibrates an order of magnitude faster. As such, Stephens and Keeling concluded that deep anoxia would not result from the effect of sea ice on the air-sea gas exchange of O_2 as this effect would be small. The storage of carbon sequestered by the biological pump would be enhanced, without need for a "strengthening" from increased productivity brought about by changes in nutrient concentrations or the efficiency of nutrient utilisation.

In the early 1990s, emphasis changed from a purely scientific quest for understanding the past and present ocean-climate system, to verifying models used for the Intergovernmental Panel on Climate Change modelling of the climate under different

high CO_2 emission scenarios. The Paleoclimate Modelling Intercomparison Project (PMIP) started alongside the already existing Coupled Model Intercomparison Project (CMIP). The impetus for PMIP was to understand and assess how different models behaved in paleoclimate conditions, hoping this may garner both greater understanding of drivers of different climate states, and to verify the fundamental processes needed to model different climate states as paleoclimate conditions were increasingly constrained by proxy data [46]. If models could produce good representations of both paleoclimate and modern ocean conditions, this would increase the confidence that the modelling of high CO_2 scenarios was also accurate. Different versions of PMIP boundary conditions were also developed to reflect the growing bodies of paleoclimate proxy data. As the LGM is the most recent, relatively stable past climate state, it gains considerable importance within PMIP studies as a broad array of geochemical data have been collected globally. The application of boundary conditions and geochemical data developed by the paleoclimate community has allowed geochemists and modellers to hypothesise why global CO_2 dropped during this period, and to better understand the drivers of oceanic CO_2 storage under different climate states.

The interplay of biological and physical processes within the ocean, and in connection with the atmosphere and sediments, is a complex and nonlinear system that at times can seem counterintuitive. The numerical modelling of these processes allows for better understanding of these systems and how different processes interplay. The major changes that have been shown to contribute to LGM carbon storage changes are: more sluggish global ocean circulation [8, 14, 15], lower global average temperature and a change in the meridional temperature gradient [47, 48], changes in the strength and pattern of winds which also contributes to changes in iron fertilisation of different ocean regions [38] and increased distribution of sea ice by 50% [49]. Increased sea ice and glaciation lowered sea level by $\sim$110m which accounts for the higher salinity and nutrient concentrations in the LGM ocean [34].

2.2 Reconstructing LGM O_2 concentration changes

Deoxygenation of the oceans is often associated with warmer greenhouse climates in the geological record (*eg* [50]). This is occurring in the oceans today with expansion of Oxygen Minimum Zones driven by reduced solubility in warmed waters, and thermal stratification which reduces deep ocean ventilation [51]. In the cooler LGM climate, the surface ocean was more oxygenated due to the temperature-driven solubility, however, paleoproxies have demonstrated widespread deep and intermediate depth deoxygenation.

A number of geochemical techniques have been developed over the last three to four decades that are based on redox properties of various elements at the bottom water-sediment interface. For these techniques to be useful, geochemists require a good handle on the geochemical properties of those elements that are sensitive to redox changes within the range seen over oxic, suboxic and anoxic seawater and sediment environments. With the advent of increasingly precise and accurate mass spectrometry-based techniques in the late 1980s, the geochemical behaviour of these elements could be effectively applied to the development of reliable paleo-oceanographic seawater O_2 proxies. Nonetheless, it needs to be recognised that these techniques have limitations and particular windows of O_2 concentration within which they can be applied; many of these techniques are only applicable in low O_2 environments ($<\sim$50 μmol/kg), limiting the geographic scope of their application.

A qualitative technique frequently used solely or in concert with other O_2 proxies is the measurement of authigenic uranium (Au-U). Au-U is the excess uranium (IV) that accumulates in suboxic sediments due to the precipitation of this reduced uranium species into an insoluble state [52]. The rate of accumulation of Au-U into sediments is dependent on the porewater uranium concentration gradient, which itself depends on the nonlinear interaction between bottom water O_2 concentration, the export flux of remineralisable organic matter to the overlying bottom waters and sediment focusing [52]. As such, the qualitative estimation of bottom water O_2 changes between the LGM and present using Au-U requires application of additional paleoproductivity proxies (such as opal flux, and protactinium and

thorium). This method was thought to only be applicable in regions with large fluxes of remineralisable organic matter [53], however, when measured with other redox sensitive trace elements (such as manganese, vanadium, zinc and nickel), it has been shown to indicate relative deoxygenation in low productivity environments resulting from ventilation, rather than productivity, changes [54], and is an area of ongoing research [55]. Multi-proxy analyses in the Arabian Sea have indicated a 3 ppm shift in Au-U occurs at $\sim$30μmol/kg, however, this threshold may not be applicable to other ocean basins [56]. Additionally, absence of an Au-U enrichment signal does not imply an absence of previous deoxygenation as subsequent re-oxygenation of overlying bottom waters can dissolve Au-U in the sediments [57, 58]. Despite these limitations, this qualitative method has been applied extensively, particularly in the deep and intermediate equatorial Pacific, providing strong qualitative evidence of LGM deoxygenation [53, 54, 57–59].

More recently, techniques have been developed using foraminifera geochemistry with the hope of producing (semi-)quantitative measures of glacial-interglacial O_2 changes. These techniques are necessarily developed and calibrated using forams in the modern ocean. This can create challenges due to shifts in species abundance and assemblages between the LGM and today limiting the regions in which the techniques can be applied [60, 61].

A semi-quantitative method is the measurement of iodine-to-calcium (I/Ca) ratios in calcitic foraminifera. This ratio is altered by the redox-driven shift of iodate (IO_3^-) and iodide (I^-) concentrations in seawater. Shifts in the proportion of iodate in seawater results in variation in the proportion of carbonate ion replacement by iodate in the calcite tests of foraminifera creating a positive linear trend with increasing seawater O_2 concentration [62]. This method has been applied to modern day foram species [62] and to species found in LGM sediment samples that were calibrated using the same species present today across a range of O_2 concentrations [60, 63]. Unfortunately, this I/Ca correlation with O_2 is only seen at O_2 concentrations below 50 μmol/kg. As such, this method is semi-quantitative as it can only be applied quantitively below, and qualitatively above, 50 μmol/kg [60].

A quantitative method with a larger O_2 range than the I/Ca method involves the measurement of $\delta^{13}C$ in epibenthic (near sediment surface) and deep infaunal (near porewater anoxic threshold) foraminifera species. This method uses the observed relationship between porewater $\delta^{13}C$ and bottom water O_2 concentrations [64]. The porewater $\delta^{13}C$ gradient of glacial sediment samples was observed through measurement of benthic foraminifera and epifaunal foraminifera living in the underlying sediment during the LGM so that bottom water O_2 concentration could be reconstructed [65]. The range over which a clear linear trend is seen is between 50 and 235 μmol/kg. This technique has been applied to glacial and preindustrial sediments, demonstrating deep ocean deoxygenation [61, 65, 66]. With any technique that involves incorporation of isotopic species by a living organism, 'vital effects' of the organism can shift isotopic ratios. This creates uncertainty as does variation between microhabitats of species, as well as differences in porewater gradients under different climate conditions, and all are potential sources of error [66, 67]. Additionally, measurements of multiple bottom water O_2 proxies at the same site have confirmed that the $\delta^{13}C$ difference in benthic and epifaunal forams may be affected by local export production, complicating how confidently the results may be applied [58, 64].

Other new techniques include the semi-quantitative calibration between the preservation of lipid biomarkers of major phytoplankton groups in sediment and bottom water O_2 [7]. This has been applied in the Eastern Equatorial Pacific demonstrating glacial deoxygenation consistent with previous studies. The study of pore density on deep-sea benthic foraminifera shells has been quantitatively calibrated to O_2 conditions [68] but is yet to be applied over glacial-interglacial cycles.

In the context of glacial-interglacial shifts, O_2 proxies that provide quantitative changes in low O_2 regions means much of the ocean cannot be well reconstructed, and it cannot be assumed that the very low O_2 regions represent the magnitude of O_2 changes globally, despite some back-of-the-envelope type analyses that do make this assumption (*eg* [7, 69]). Until more data is collected with quantitative methods such as the epibenthic-infaunal $\delta^{13}C$ technique that allow for glacial-interglacial

changes of O_2 in the 50 to 250 μmol/kg range, the extensive qualitative glacial-interglacial changes observed in low O_2 regions cannot be confidently extrapolated to be representative of other regions of deep and intermediate depth ocean.

2.3 Modern O_2 and AOU measurements

O_2 and CO_2 are closely coupled through photosynthesis and respiration reactions. O_2 is produced during photosynthesis where the macronutrients carbon, phosphate and nitrate are converted into organic matter, along with micronutrients such as iron. Carbon is expressed as CO_2 in Eq. 2.1 but is more generally obtained by most organisms from seawater as bicarbonate ions which are converted to CO_2.

$$PO_4H_3 + \quad \alpha NO_3H + \beta CO_2 + \lambda H_2O = (CH_2O)_\beta (NH_3)_\alpha PO_4H_3 + \gamma O_2 \quad (2.1)$$

$$where, \qquad R_{N:P} = \alpha = 16 \pm 1 \quad (2.2)$$

$$R_{C:P} = \beta = 117 \pm 14 \quad (2.3)$$

$$R_{-O2:P} = \gamma = 170 \pm 10 \quad (2.4)$$

The relationship between O_2 and carbon through the formation and respiration of organic matter (Eq. 2.1) means that O_2 can be a useful indicator of changes in ocean carbon storage. To estimate the amount of organic carbon remineralised in the deep ocean the parameter called Apparent Oxygen Utilisation (AOU) is used, both in models and in observations. AOU is the difference between the theoretical O_2 saturation concentration (calculated using *in situ* temperature,θ, and salinity, S) and the observed O_2 concentration (Eq. 2.5). Assuming that surface waters are at equilibrium with the atmosphere before subduction to depth, AOU will reflect the amount of O_2 consumed during aerobic respiration of sinking organic matter and can be used to calculate respired carbon or phosphorus using the Redfield ratios between carbon, phosphorus, and O_2, as shown in Eq. 2.1, using ratio ranges determined by Anderson and Sarmiento [5], and the appropriate stoichiometric value of λ necessary to balance the specific C:N:P:-O_2 stoichiometry values.

$$AOU = O_{2,sat}(\theta, S) - O_2 \tag{2.5}$$

When estimating remineralisation, AOU is used with stoichiometric ratios of phosphate and carbon production, rather than with nitrate, as $R_{-O2:P}$ is more robust than $R_{-O2:N}$ and $R_{C:N}$ [5]. Estimates of these Redfield ratios vary depending on methods used (*eg* linear regression [70] or inverse model [5]). These estimates show approximately constant ratios across depth and ocean basins for regeneration of nutrients below 400 m. Due to the importance of Redfield ratios in estimates of global carbon storage and O_2 utilisation, their variability has been recently explored, focusing on variability across ocean basins and latitude, seasonality, and ecosystem composition. Galbraith and Martiny [21] proposed a predictive framework which they deem a necessity for modellers who wish to incorporate variable stoichiometry into global biogeochemical models. Their model compared well with observations (*eg* [71])

Other models have incorporated flexible ecosystem composition changes among phytoplankton groups that are driven by changes in nutrient distributions resulting in an increase in the carbon-to-phosphate ratio of phytoplankton and subsequent increase in CO_2 drawdown [72]. In the context of glacial ocean models, this has only been studied once to date, with enhanced carbon storage observed in the flexible carbon-to-phosphate stoichiometry simulations compared to the fixed stoichiometry simulation [73]. The effect of these stoichiometric changes on O_2 consumption were not evaluated.

The primary drivers of O_2 concentration changes are the production of O_2 during photosynthesis, the consumption of O_2 during aerobic respiration of organic matter, and temperature and salinity that affect O_2 solubility in the surface ocean. In the ocean today, the warming climate is causing Oxygen Minimum Zone expansion and temperature-driven surface deoxygenation, both of which are major stressors on marine ecosystems [74]. Because of the more rapid air-sea gas equilibration of O_2 than CO_2, most papers dealing with the relationship between O_2, AOU and carbon storage work with the assumption that O_2 in surface waters will have negligible

disequilibrium, especially when compared to carbon disequilibrium (*eg* [10]); that is, preformed O_2 can be estimated reliably from the O_2 saturation value calculated from *in situ* temperature and salinity. This is despite evidence from the modern ocean showing high latitude O_2 disequilibrium in deep and intermediate waters formed in the Southern Ocean [24, 75] and the North Atlantic [76].

The importance of O_2 disequilibrium on AOU-based estimates of carbon respiration was succinctly outlined by Ito and Follows [25]. They differentiated between True Oxygen Utilisation (TOU) and AOU in a coupled ocean general circulation-biogeochemical model by including preformed O_2 as a conservative, passive tracer. This allowed calculation of both AOU and TOU in their simulations of the preindustrial ocean, from which systemic overestimation of interior respiration was shown to result when using AOU. The primary causes of O_2 disequilibrium were identified as the prevention of gas exchange due to sea ice, upwelling of high latitude waters that were O_2-undersaturated due to respiration in the ocean interior, and meridional temperature gradient causing cold, high latitude waters to be incompletely saturated before subduction. The magnitude of O_2 disequilibrium is also expected to be larger in the Southern Ocean than the North Atlantic as upwelled, O_2-poor waters have less time in contact with the atmosphere before subduction [77]. These results were significant for modelling studies as solubility- and wind-driven O_2 air-sea gas exchange is similarly parameterised across multiple models using empirical relationships [78].

The O_2 disequilibrium was shown to be fairly constant across isopycnal surfaces, so Ito and Follows proposed that inert gases could be used to track and correct for this effect [25]. Duteil et al [26] presented an observationally-based method to evaluate O_2 utilisation more accurately to correct this overestimation, which they also demonstrated to be present in six coupled circulation-biogeochemical models. Their method used the assumption that O_2 disequilibrium is mostly constant along isopycnals. By determining the magnitude of O_2 disequilibrium near the surface where isopycnals outcrop an estimate of preformed O_2 for the isopycnal was made that could be used instead of theoretical O_2 saturation value.

Their estimates of O_2 utilisation were closer to TOU than when AOU was instead used, with global estimates of O_2 utilisation (and therefore remineralised carbon) being ∼25% lower than AOU.

The effect of both carbon and O_2 disequilibrium in glacial-like conditions was investigated by Eggleston and Galbraith [79] using a coupled climate-ocean-biogeochemical model. The tracing of preformed O_2 allowed for total O_2 disequilibrium to be traced by taking the difference from the saturation O_2 values calculated using temperature and salinity. These were assessed under different climate conditions including a glacial-like condition driven by radiative forcing and orbital changes, and included experiments that also included glacial ice sheet cover and dust (iron) fertilisation. Interglacial-like and glacial-like conditions were explored but a full simulation was not included that could have showed the combined effects of preindustrial or LGM sea ice cover, iron fertilisation and temperature-dependent changes to organic matter remineralisation. The O_2 disequilibrium results across the various experiments were not shown in detail, however, the authors note that in the cold climate state simulations there is significant O_2 disequilibrium which becomes sensitive to sea ice cover in the Southern Ocean as the model state is more similar to the LGM climate, despite the more rapid equilibration time of O_2 than CO_2. Additionally, they observed that estimates of carbon storage resulting from organic matter were overestimated when using AOU despite the model results that indicated increased glacial ocean ventilation should have reduced organic matter production. The authors note a number of possible causes of these conflicting results, including the effect of negative O_2 disequilibrium causes an overestimation of organic matter remineralisation, a result that would also have implications for how O_2 proxies are applied to estimates of carbon storage.

2.4 UVic-MOBI2.0 biogeochemical model and disequilibrium

The University of Victoria (UVic) ocean general circulation model was coupled with the Model of Ocean Biogeochemistry and Isotopes version 2.0 (MOBI2.0)

biogeochemical model for the research presented in this thesis. Reconstructions of increased salinity brought about by lowered sea level and colder temperature can be used to set boundary conditions for models seeking to reproduce the LGM. Temperature fields that incorporate a shift in the poleward gradient have been developed that can be implemented into models (*eg* [80]). Cooler temperatures have also been shown to deepen the remineralisation depth [81], and was parameterised in the model. According to reconstructions of radiocarbon ($\Delta^{14}C$), the deep ocean was more isolated from the atmosphere in the LGM than the preindustrial ocean, which could account for greater deep ocean carbon storage as there was less air-sea gas exchange [8, 82] particularly in the Southern Ocean where radiocarbon levels were very low [15]. Additionally, various geochemical tracers can be included depending on the phytoplankton biology included in a given biogeochemical model. The MOBI2.0 includes calcifying and non-calcifying phytoplankton and diazotrophs which are parameterised to include the cycling of carbon and nitrogen isotopes for $\delta^{13}C$ and $\delta^{15}N$ analyses [22, 83]. Reconstruction of LGM circulation, particularly of the structure of the Atlantic Meridional Overturning Circulation (AMOC), is an area of considerable study and also of contradicting results [84]. Using the biological tracers $\delta^{13}C$ and $\delta^{15}N$ of benthic foraminifera—tracers that contain information about air-sea gas exchange and biological activity, and nutrient utilisation, respectively—and radiocarbon ($\Delta^{14}C$) as a ventilation tracer, Muglia and Schmittner [80] found a circulation pattern characterised by a weak and shallow AMOC and increased fraction of Antarctic Bottom Water resulted in the best fit with available data. These results were in contrast to studies using ^{231}Pa/^{230}Th and sediment grain size data, which suggested a shallower AMOC without weakening of circulation [85, 86], but in agreement with other studies suggesting weaker overturning circulation in the LGM Atlantic using silt grain size [87]. To achieve full reconciliation of $\delta^{13}C$, $\delta^{15}N$ and $\Delta^{14}C$, Muglia and Schmittner [80] incorporated high Southern Ocean iron fluxes using glacial dust data from Lambert et al. [88], and described in a previous model paper [89].

In a study of LGM ocean carbon storage by Khatiwala [20], the role of carbon air-sea gas disequilibrium was included in determining the major drivers of deep ocean carbon storage in the coupled UVic-MOBI2.0 model. By running the MOBI2.0 biogeochemical model offline using the Transport Matrix Method [90, 91] additional tracers including preformed DIC, saturated preformed DIC and preformed phosphate could be included without significant lengthening of model run times compared to an online model. This allowed for a full decomposition of the carbon disequilibrium system. Perturbation experiments in which an LGM condition was used to perturb the steady-state preindustrial ocean, allowed for observation of the separate roles of LGM temperature, salinity, circulation, iron fertilisation, and sea ice expansion on the drawdown of atmospheric pCO_2. Circulation changes and sea ice are often considered important for the global climate state and the drawdown of glacial atmospheric pCO_2, however, it was not of most significance in the experiments [20]. This result was interesting for circulation as the experiment was performed using the LGM circulation field which reduced export production due to reduced upwelling, but maintained preindustrial temperature and salinity conditions, a separation that is not generally performed. The role of these mechanisms in O_2 air-sea gas exchange and biological consumption was therefore of interest for O_2 to see if the results would be consistent between the carbon and O_2 systems. Instead, temperature (with preindustrial circulation) and iron fertilisation were found to be the main drivers of glacial carbon deep ocean storage through enhancement of physically- and biologically-driven disequilibrium, respectively.

The results of Khatiwala [20] demonstrated the importance of carbon disequilibrium in enhancing LGM carbon storage despite an overall reduction of the soft-tissue carbon export, and the observation of both O_2 disequilibrium and widespread LGM deep ocean deoxygenation provide the impetus for the work presented here. The focus of this thesis is understanding the storage of O_2 in the preindustrial ocean, and during the Last Glacial Maximum (LGM), by rigorously quantifying the magnitude and role of disequilibrium O_2, and the effect this O_2 component has on estimates of ocean carbon storage.

Chapter 3

Deoxygenation in the Last Glacial Maximum Ocean

The content of this chapter, thesis abstract and Appendix 1 has been published in *Nature Geoscience* by Cliff, Khatiwala, and Schmittner [92] (DOI: 10.1038/s41561-020-00667-z) and is reformatted here from the accepted version. EC and SK designed research; AS developed model used; SK ran climate models including creation of appropriate transport matrices; EC analysed data, generated results, and wrote the paper with input from SK and AS.

Contents

3.1 Introduction

O_2 is fundamental for life in the ocean, and is intrinsically connected with the cycling of carbon through photosynthesis: CO_2 is fixed and O_2 produced by phytoplankton in the surface ocean, and O_2 is consumed and dissolved inorganic carbon (DIC) released when organic matter is broken down by microbial respiration throughout the ocean. This transfer of carbon to the deep ocean is termed the "soft-tissue pump". O_2 can thus be a powerful tool to understand the cycling and storage of respired carbon in the ocean, the quantification of which is important for answering fundamental questions of carbon cycling under different climate states.

The Last Glacial Maximum (LGM; ∼20,000 years before present) is the most recent example of a relatively stable, different climate state. This was a period when global mean ocean temperatures were 2.5°C colder than preindustrial times, and atmospheric CO_2 was ∼90 ppm lower [8, 9]. The deoxygenation of the deep ocean relative to the preindustrial has been observed globally using a variety of O_2 proxies from seafloor sediments [6, 58]. These results have been used to support the hypothesis that deep ocean carbon storage in the LGM was the result of a stronger or more efficient soft-tissue carbon pump [6, 7, 13, 21, 57, 93], which could partially explain the reduction of atmospheric CO_2 during glacial periods [8, 9]. It was recently demonstrated [20] with an observationally-constrained model that glacial carbon storage in the deep ocean was enhanced by air-sea disequilibrium of CO_2 caused by temperature changes and iron fertilization, while changes in circulation and sea ice extent, previously regarded as the primary drivers, played a minor role. Importantly, atmospheric CO_2 was reduced through increased deep ocean carbon storage, even as export production in the modeled glacial ocean decreased. However, deep ocean O_2 still decreased in the model. Here, we show that air-sea disequilibrium of O_2 can be a substantial part of the O_2 budget, potentially decoupling O_2 from biological carbon storage and confounding efforts to use it as a proxy to reconstruct past variations in the efficiency of the biological carbon pump.

Due to the more rapid air-sea gas equilibration timescale of O_2 relative to CO_2 (a few weeks versus ∼a year [23]), O_2 disequilibrium has often been considered a

minor component of the modern and LGM O_2 budget [10, 21, 77]. In the modern ocean, observations show summertime O_2 oversaturation caused by photosynthesis, while wintertime undersaturation at high latitudes is driven by heat fluxes, extensive sea ice cover and wind-driven upwelling of oxygen-depleted deep waters [25, 76] (Fig. 3.1). The deep ocean is supplied with O_2 through subduction at high latitudes in the wintertime, when cold, dense water masses develop, following deep convection and sea ice formation. The effect of disequilibrium may be greater in the Southern Ocean as oxygen-depleted intermediate and deep waters upwelling to the surface there have a shorter surface exposure time than those in the North Atlantic [77]. The propagation of undersaturated waters from the Southern Ocean into the interior, a phenomenon supported by observations [24], could have an especially large impact on the ocean's O_2 inventory because a large fraction of the deep ocean is ventilated from the Southern Ocean [94]. The ocean model used in this study shows reasonable agreement with observed surface O_2 saturation (Fig. 3.1). Modeled wintertime disequilibrium in the northern North Atlantic is larger than observed, which likely leads to overestimated disequilibrium in North Atlantic Deep Water in the model. Large model-data differences in the Arctic are based on very sparse observations there, which may be influenced by sampling biases in conditions without or with thin sea ice because research vessels are limited in accessing regions with thick sea ice cover. However, in the high latitude wintertime Southern Ocean, an important region of deep and bottom water formation, the (few) Southern Ocean wintertime measurements available show greater undersaturation than the model.

The Southern Ocean is known to be important in the storage of glacial CO_2 [8, 93] and the mechanisms affecting LGM carbon disequilibrium have recently been modeled [20]. A number of modelling studies have shown that O_2 disequilibrium can be non-neglible [25, 26] but a study of mechanisms affecting LGM deoxygenation is lacking. While some studies have assumed that O_2 disequilibrium does not vary greatly between the modern and LGM climate states [21, 77], others have suggested that like carbon disequilibrium, O_2 disequilibrium could be larger in the LGM [7, 79]. Here, we apply a comprehensive method of decomposition of O_2 to quantify

the magnitude of O_2 disequilibrium and investigate the processes driving glacial deoxygenation. This approach allows the effect of air-sea disequilibrium to be tracked through model simulations, and for physical and biological effects to be separated. The method is applied to biogeochemical fields simulated by two different configurations of an Earth System Model (UVic 2.9 ESCM [95]) coupled to the Model of Biogeochemistry and Isotopes (MOBI) [22] using the Transport Matrix Method [90, 91, 96]. The configurations represent preindustrial control (PIC) and LGM conditions, and were tuned to a suite of modern biogeochemical and LGM sedimentary isotope (δ^{13}C, $\Delta^{14}C$ and δ^{15}N) records [80] (see Methods).

3.2 O_2 decomposition analysis

To accurately track the cycling of O_2 in the model we express the total O_2 content of the ocean as a sum of "preformed" ($O_{2,\mathrm{pre}}$) and "soft-tissue" ($O_{2,\mathrm{soft}}$) components [25, 26] (Fig. 3.2; Eq. 3.1; see the Supplement for further details). A preformed tracer is a tracer whose value is set at the surface of the ocean, in the case of $O_{2,\mathrm{pre}}$ the simulated O_2 field at the surface of the ocean, and is subsequently transported passively and conservatively into the interior by the circulation. $O_{2,\mathrm{soft}}$ is the O_2 consumed when organic matter is broken down, and accumulates as a deficit in the ocean interior, while regenerated dissolved inorganic carbon (DIC), nitrate and phosphate accumulate (Fig. 3.2).

$O_{2,\mathrm{soft}}$ is calculated from respired carbon (C_{soft}) as $O_{2,\mathrm{soft}} = (-1/R_{\mathrm{C:-O_2}}) \times C_{\mathrm{soft}}$, where $R_{\mathrm{C:-O_2}}$ is a constant carbon-to-oxygen stoichiometric ratio. We diagnose $C_{\mathrm{soft}} = R_{\mathrm{C:P}} \times PO_{4,\mathrm{reg}}$, where $R_{\mathrm{C:P}}$ is the carbon-to-phosphorus stoichiometric ratio and regenerated phosphate ($PO_{4,\mathrm{reg}}$) is calculated as the difference between the concentrations of *in situ* phosphate and an explicitly simulated preformed phosphate tracer. Unlike nutrients, both O_2 and CO_2 can exchange with the atmosphere at the air-sea interface, affecting the preformed O_2 and DIC pools.

We further decompose preformed O_2 into $O_{2,\mathrm{eq}}$, the theoretical O_2 concentration of a water parcel in solubility equilibrium with the atmosphere, and $O_{2,\mathrm{dis}}$, the

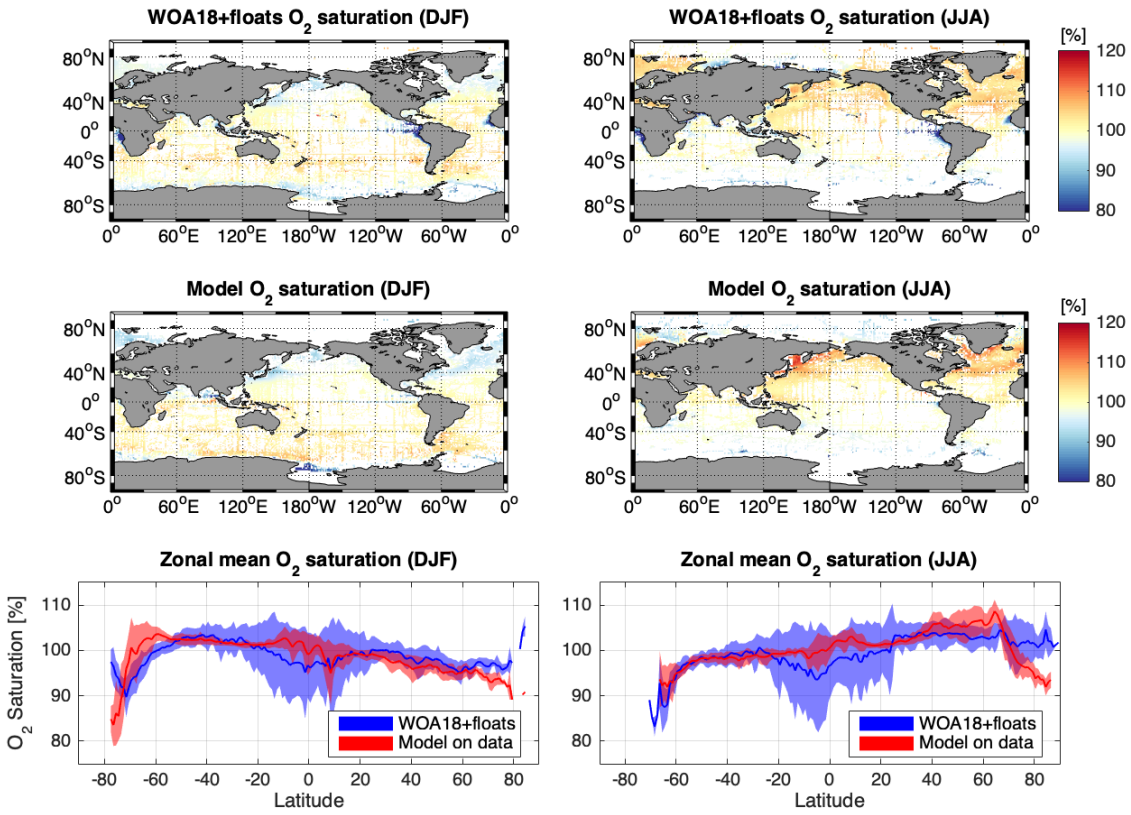

Figure 3.1: Comparison of surface O_2 saturation from a compilation of World Ocean Atlas 2018 (WOA18; [97]) and float data (University of Washington Argo O_2 reanalysis [98], and quality-controlled data from the SOCCOM program [99]). Data were spatially binned into 1°×1°WOA grid boxes, and a seasonal climatology was made by binning data temporally by month. Grid boxes without any measurements were discarded. Results shown here are for northern hemisphere winter/southern hemisphere summer (December-January-February; left) and northern summer/southern winter (June-July-August; right). Surface O_2 saturation values are shown for observations (top) and the model preindustrial control simulation interpolated to the locations where observations are available (middle row). The bottom row shows a comparison of zonal mean surface O_2 saturation in the observations and model at the location of observations with one standard deviation of the zonal data shaded. Note that observations for the Southern Ocean are sparse, particularly in the winter months.

disequilibrium component that leads to deviation of $O_{2,\mathrm{pre}}$ from $O_{2,\mathrm{eq}}$. O_2 disequilibria at the surface are driven by both sea surface temperature (SST) gradients and upwelling of waters depleted in O_2 due to biological consumption [25, 79]. To distinguish between these mechanisms, we carry out a parallel simulation for each experiment in which biogeochemical processes are switched off. By taking the

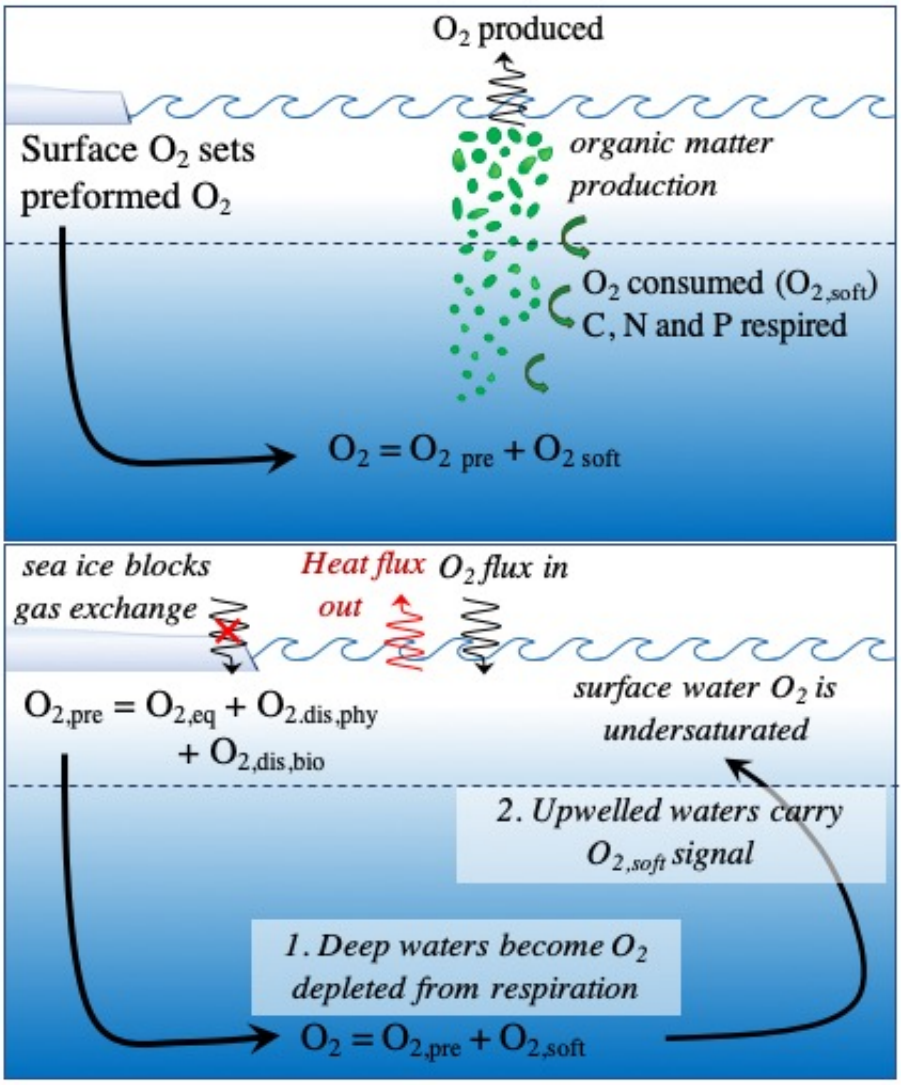

Figure 3.2: Schematic of the O_2 decomposition used in this study. Top panel shows the standard decomposition of O_2 into preformed O_2 ($O_{2,\mathrm{pre}}$), set at the surface, and $O_{2,\mathrm{soft}}$, O_2 consumed during respiration of organic matter (which is therefore negative). The sum of these terms gives total O_2. The bottom panel shows the extended decomposition that incorporates surface disequilibrium which causes deviation from the equilibrium preformed concentration ($O_{2,\mathrm{eq}}$). Physical disequilibrium ($O_{2,\mathrm{dis,phy}}$) is caused by surface heat fluxes. Biological processes can also cause disequilibria ($O_{2,\mathrm{dis,bio}}$) by photosynthesis at the surface, creating a positive disequilibrium, or as a result of the upwelling of waters depleted in O_2 due to respiration, leading to a negative disequilibrium. Waters upwelling in the Southern Ocean have a short surface exposure time so can have significant $O_{2,\mathrm{dis,bio}}$, which may be enhanced by sea ice blocking gas exchange.

difference between the full physical-biogeochemical and the physics-only simulations, we can distinguish between biological and physical contributions to $O_{2,dis}$. Physical disequilibrium, $O_{2,dis,phy}$, occurs when waters moving poleward do not equilibrate fully as they lose heat. Biologically-mediated O_2 disequilibrium, $O_{2,dis,bio}$, occurs when waters depleted in O_2 from either $O_{2,soft}$ or $O_{2,dis,bio}$ are entrained or upwelled to the surface. Once at the surface the part of this deficit that is not replenished through air-sea gas exchange is relabelled as $O_{2,dis,bio}$ and becomes part of the preformed O_2 pool that is resubducted into the ocean interior. $O_{2,dis,bio}$ is calculated as the difference in $O_{2,dis}$ between the full and physics-only simulations. This is illustrated in Fig. 3.2. In summary, the concentration of O_2 at any point in the ocean can be decomposed as Eq. 3.1:

$$O_2 = \underbrace{O_{2,eq} + O_{2,dis,phy} + O_{2,dis,bio}}_{O_{2,pre}} + O_{2,soft} \tag{3.1}$$

We note that $O_{2,soft}$ is negative, as generally are $O_{2,dis,phy}$ and $O_{2,dis,bio}$, i.e., they reduce the O_2 inventory of the ocean from $O_{2,eq}$. A similar approach was previously applied to carbon using the same model [20], allowing for comparison of O_2 and carbon.

3.3 O_2 distribution in the preindustrial and LGM

The O_2 inventory and its components for the PIC and LGM are shown in Table 3.1 and in Fig. 3.3. In the preindustrial configuration total ocean O_2 content is 266 Pmol O_2 (global mean concentration of 196 mmol m^{-3}), similar to estimates of the modern ocean inventory (227 Pmol) [51] and within the range of CMIP5 models (136-231 mmol m^{-3}) [100]. As expected, $O_{2,eq}$ is the largest component; all other components reduce the inventory so that total O_2 is 40% of the equilibrium value. Two thirds of the reduction is due to consumption during respiration ($O_{2,soft}$), with the remaining decrease due to disequilibrium, of which 80% is biologically-mediated ($O_{2,dis,bio}$). The spatial distribution and magnitude of $O_{2,dis}$ (Fig. A.2) are similar to those in a previous study [25].

Table 3.1: Results of the O_2 decomposition for PIC and LGM equilibrium runs are shown in terms of the total inventory (Pmol) and global mean concentration (mmol m^{-3}). Negative values indicate a deficit of O_2 resulting from incomplete equilibration or consumption during respiration. The differences between the LGM and PIC inventory values are also shown, with positive (negative) values indicating more (less) O_2 in the LGM than PIC.

	O_2	$O_{2,eq}$	$O_{2,dis,phy}$	$O_{2,dis,bio}$	$O_{2,soft}$
PIC (Pmol)	266	458	-12	-49	-127
PIC (mmol m^{-3})	196	337	-9	-36	-94
LGM	233	482	-9	-132	-104
LGM (mmol m^{-3})	172	355	-7	-97	-77
LGM-PIC (Pmol)	-33	+24	+3	-83	+23
LGM-PIC (mmol m^{-3})	-24	+18	+2	-61	+17

The glacial ocean has ∼12% less O_2, consistent with proxy-based reconstructions that show widespread deep ocean deoxygenation (Fig. 3.3; [6, 7, 21, 58–61, 63, 65, 66, 101, 102]). The majority of available proxy data are qualitative, indicating whether O_2 was higher or lower in the LGM (20-22ka BP) relative to the Holocene (5-10ka BP). The model captures the general pattern of upper ocean oxygenation in LGM and deoxygenation in the deep ocean relative to the PIC, although may be underestimating the full magnitude of deep ocean deoxygenation (see Supplement for further comparison of model and reconstructions).

LGM O_2 decreases despite the cooler temperatures that enhance O_2 solubility and thus $O_{2,eq}$ (by ∼5%) (Figs. 3.3, A.6). O_2 is also enhanced by increases in $O_{2,dis,phy}$ and $O_{2,soft}$, both of which are less negative in the LGM (by ∼25% and ∼20%, respectively). Globally, export production in the LGM simulation is reduced causing this $O_{2,soft}$ increase. While there is no observational estimate of global export production during the LGM, estimates do exist in some regions [103] and the model captures these variations reasonably well (Fig. A.3). The only component of the O_2 budget that drives glacial deoxygenation is $O_{2,dis,bio}$, which nearly triples in the glacial ocean simulation (to -132 Pmol), overwhelming increases brought about by changes due to physical processes and organic matter export. The decomposition of O_2 into its physical and biological components enables a

more complete appreciation for the glacial-interglacial difference in O_2 distributions that has not been demonstrated before. That the decline in O_2 during the LGM is driven by biologically-mediated disequilibrium is a novel finding.

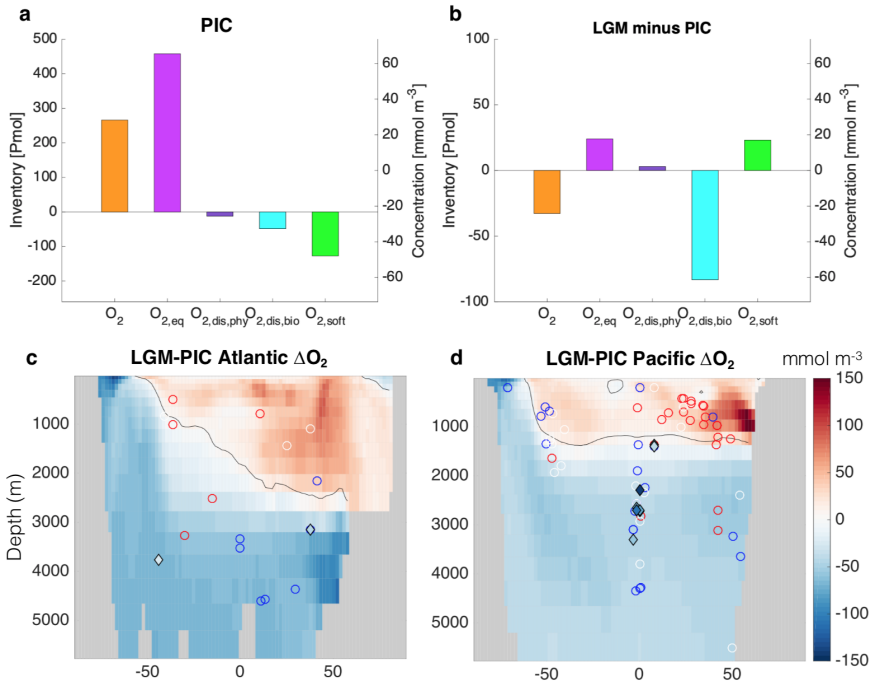

Figure 3.3: The components of O_2 in the preindustrial (PIC) and LGM relative to the PIC. Oxygen decomposition for the preindustrial control (PIC) equilibrium simulation (a) and the difference between the Last Glacial Maximum (LGM) and PIC equilibrium simulations (b) are shown as inventory values in Pmol O_2 and mmol m^{-3}. The equivalent deep ocean inventory decomposition plots are in Fig. A.5. Zonal mean sections of LGM-PIC ΔO_2 are shown for the Atlantic (c) and Pacific (d) oceans. Proxy-based reconstructions of ΔO_2 from the LGM to Holocene have been included. Blue (red) circles indicate a qualitative decrease (increase) in O_2 from the holocene (5-10 kyr bp) to the LGM (20-22 kyr bp) [6, 7, 21, 59, 61, 63, 66, 101]. Diamonds represent a quantitative O_2 change [58, 61, 65, 102] using results of the infaunal-epifaunal foraminifera $\delta^{13}C$ method that were within the range of a previously published calibration [65] and are shaded using the same color scale as the color bar. The quantitative data point shown in the southern Atlantic was calculated using the modern O_2 concentration at the core site as data was not available for the Holocene [66] and recalculated per ref. [104]

3.4 Drivers of LGM deoxygenation

To understand the mechanisms behind glacial ocean deoxygenation, a series of perturbation experiments was performed where a single parameter (temperature, circulation, sea ice or iron fertilization) in the preindustrial configuration was

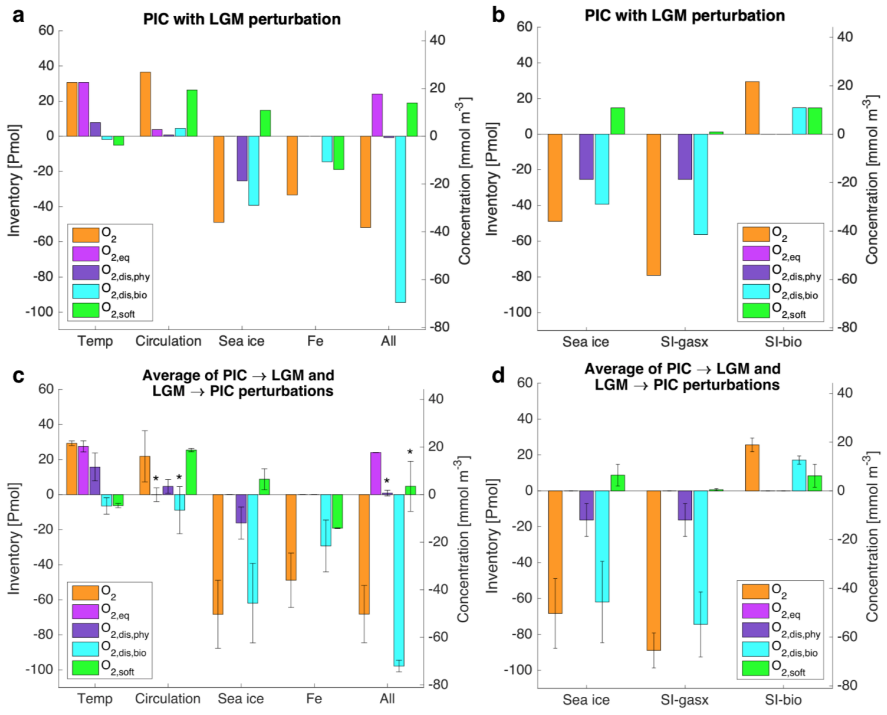

Figure 3.4: Top row: Response of PIC O_2 components to LGM perturbations. (a) Change in inventory due to a perturbation in circulation; sea ice; temperature; iron; all perturbations in which LGM temperature, circulation, sea ice, iron fertilization, salinity (1-PSU increase consistent with 110 m sea level drop) and winds were used to perturb the PIC. (b) Change in inventory due to perturbation of sea ice; SI-gasx: effect of sea ice on O_2 gas exchange; SI-bio: sea ice effect on light limitation for biology. Bottom row: Assessment of robustness of response of O_2 components to perturbations. Vertical bars are the difference between the PIC to LGM and LGM to PIC experiments (Eq. A.9) and indicate whether the response is of the same or opposite sign in the two directions (see Supplement for details). The vertical lines are the sum (Eq. A.10) and show the average magnitude of the perturbation for the two experiment sets, such that if a line crosses the x axis, it implies a non-robust response to the perturbation. Those experiments are marked with an asterisk. (c) and (d) Changes due to perturbations corresponding to those in (a) and (b), respectively.

changed to its LGM condition and the model run to equilibrium. An additional "All" experiment was carried out where these parameters (and salinity) were all changed to the LGM condition. (The "All" experiment does not exactly reproduce the LGM equilibrium simulation as it still uses the PIC conditions for light, freshwater fluxes and subgrid bathymetry, which affects sedimentary release of organic carbon.) The differences between the LGM perturbation and the PIC are shown in Fig. 3.4 for the inventories of the O_2 components. These differences are also shown as zonal means of the Atlantic and Pacific basins (Figs. A.10- A.22). To probe the

dependence of the response on the base state of the model [79], a "reverse" set of experiments was also run where the PIC condition was used to perturb the LGM state (see Figs. A.11- A.23 for comparison).

In the LGM temperature perturbation experiment, a non-uniform temperature change consistent with reconstructions [47, 48] is imposed, which increases the ocean's O_2 inventory by 30 Pmol ($\sim$24 mmol m^{-3}). The leading order effect is an increase in $O_{2,eq}$ (by 31 Pmol) through enhanced solubility. Changes in $O_{2,eq}$ closely follow the pattern of temperature change with the largest differences seen in the North Atlantic (Fig. A.24). The LGM meridional SST gradient and heat fluxes are weakened at high-latitudes, reducing heat flux-driven undersaturation. This causes $O_{2,dis,phy}$ to become less negative in waters south of $\sim$60°S and results in a small (8 Pmol) increase in oxygen. This increase is somewhat countered by biological factors. Cooler temperatures deepen the remineralization depth [81], producing the pattern of reduced O_2 consumption in the upper ocean and increased O_2 consumption in the deep ocean seen in both the Atlantic and Pacific (Fig. A.10), leading to a global decrease (by 5 Pmol) in $O_{2,soft}$. A similar decomposition applied to carbon showed that temperature was a major cause of atmospheric CO_2 drawdown (by 45 ppm) due to enhanced solubility and physical disequilibrium [20], illustrating that carbon and O_2 disequilibrium are controlled by different processes.

Circulation in the simulated LGM ocean is characterized by a weaker (by $\sim$50%) and shallower Atlantic meridional overturning circulation. This reduces upwelling of nutrient-rich deep waters in the Indo-Pacific causing a global reduction in export production [20, 105, 106]. Thus, the primary effect of circulation changes is to increase the ocean's O_2 inventory by reducing O_2 consumption. The reduced magnitude of $O_{2,soft}$ is observed through much of the Atlantic and most strongly in the Pacific (Fig. A.12). Though a much smaller effect, $O_{2,dis,bio}$ is also reduced under LGM circulation, which may be attributed both to a smaller $O_{2,soft}$ pool and because slower overturning circulation provides more time for waters upwelled in the Southern Ocean to equilibrate before subduction. O_2 decreases in upper and intermediate North Atlantic waters due to changes in the propagation of $O_{2,eq}$

into the interior, although the net effect of changing the transport of $O_{2,eq}$ into the interior is a small increase globally.

The LGM configuration has 50% more sea ice than the PIC one such that Southern Ocean maximum (winter) cover is 3×10^{13} m^2, slightly less than reconstructions (4×10^{13} m^2) [107]. Sea ice blocks both air-sea gas exchange and penetration of light to the surface ocean. The former is expected to enhance disequilibrium, driving more negative $O_{2,dis,phy}$ and $O_{2,dis,bio}$ values as sea ice acts as a cap that prevents equilibration of O_2-depleted waters, whereas the latter reduces phytoplankton growth, and hence export production and biological consumption of O_2. To quantitatively separate these mechanisms we carried out two additional experiments in which sea ice alternatively affected only gas exchange (SI-gasx) or biology through light limitation (SI-bio) (Figs. A.16, A.18). These experiments show that air-sea gas exchange has a much larger effect than light limitation, reducing O_2 by 81 Pmol ($\Delta O_{2,dis,phy} = -25$ Pmol and $\Delta O_{2,dis,bio} = -56$ Pmol). Light limitation has a smaller and compensatory effect, increasing O_2 by 30 Pmol ($\Delta O_{2,soft} = +15$ Pmol, $\Delta O_{2,dis,bio} = +15$ Pmol). The net effect is additive, decreasing the O_2 inventory by 49 Pmol in the sea ice perturbation experiment. These changes in O_2 are largely driven by greater sea ice extent in the Southern Ocean, with decreases of over 50 mmol m^{-3} in AABW in the South Atlantic (Fig. A.14). These results are consistent with previous studies that showed the large effect of sea ice on gas exchange for $O_{2,dis}$ in the Southern Ocean [25, 79], although those studies did not separate biologically-mediated disequilibrium from physical disequilibrium. While the implementation of sea ice effects in our model is typical of other global models, it does not include polynyas and sea ice leads, which may reduce the strength of these effects as some gas exchange would still be possible and polynyas may allow for pockets of productivity. Polynyas are thought to have been present in the glacial Southern Ocean [108], although their prevalence and mechanisms of formation are not well-understood even in the modern ocean (e.g., [109]). Similarly, the inclusion of leads would allow for more equilibration in ice-covered waters. These processes may be an important

source of uncertainty for glacial-interglacial deep ocean O_2 and carbon and their inclusion should be a priority for future biogeochemical modelling studies.

Bioavailable iron fluxes to the LGM Southern Ocean (south of 35°S) are increased ten fold [80], consistent with evidence from Antarctic ice cores [49] and ocean sediment records [38]. This iron fertilization increases Southern Ocean export production. O_2 is consequently depleted due to greater consumption and enhancement of biological undersaturation ($\Delta O_{2,\mathrm{soft}} = -19$ Pmol; $\Delta O_{2,\mathrm{dis,bio}} = -14$ Pmol; Supplementary Fig. A.20). A recent study with a biogeochemical model driven by forcing fields from a coupled climate model, also examined the effect of glaciogenic iron fluxes on CO_2 drawdown and deep ocean deoxygenation in the glacial ocean [13]. They showed that high Southern Ocean iron fluxes and an increase in the ocean's nutrient inventory was associated with a third of the change in deep ocean (below 2000 m) Apparent Oxygen Utilization (the difference between theoretical saturation O_2 and observed O_2) in their LGM model (their experiment LGM_glac3% which has conditions most similar to ours). Differences in experimental design and model base states makes direct comparisons difficult, however, analysis of the changes in deep ocean O_2 content for the iron fertilization perturbation experiment provides the closest point for comparison. Our LGM iron perturbation leads to a 32 mmol m^{-3} decline in deep ocean O_2 relative to the PIC, which is comparable with the other study which recorded a 21 mmol m^{-3} change due to iron fertilization [13]. Our decomposition allows us to show that almost half of the deoxygenation brought about by iron fertilization-enhanced export production is a result of biologically-mediated disequilibrium amplifying the strength of the soft-tissue pump [77]. As the other study uses a similar gas exchange parameterization it is likely to have air-sea gas disequilibrium, although the magnitude and role of disequilibrium is not known as $O_{2,\mathrm{pre}}$ was not explicitly considered in that study.

Lastly, we consider the "All" experiment where the above perturbations were imposed simultaneously, along with a 1-PSU increase in ocean salinity corresponding to a 110 m drop in LGM sea level. The results are largely consistent with the difference between the LGM and PIC equilibrium runs (Table 3.1 and Figs. 3.3,

A.6 and A.22). The dominant cause of glacial deoxygenation is a large increase in biologically-mediated disequilibrium ($\Delta O_{2,dis,bio} = -94$ Pmol). The individual perturbation experiments suggest that this is driven by Southern Ocean sea ice and iron fertilization, which is consistent with the dipolar pattern of export production in the Southern Ocean during the LGM (Fig. A.3) [20, 103]. Despite the increase in productivity in the Southern Ocean, global productivity is reduced in the "All" experiment. Deoxygenation is partially compensated by enhanced solubility because of cooling ($\Delta O_{2,eq} = +24$), and a decrease in export production and consumption ($\Delta O_{2,soft} = +19$) due to changes in circulation. The results of the individual perturbations do not add to produce the "All" experiment result because of nonlinearities. For instance, in the Southern Ocean the interplay of expanded LGM sea ice and iron fertilization may further enhance $O_{2,dis,bio}$, while weaker latitudinal temperature gradients could reduce the effect of sea ice on $O_{2,dis,phy}$.

The "reverse" set of experiments, where PIC perturbations were imposed on the LGM state, allow us to assess the robustness of different processes in their effect on any given O_2 component. A process that elicits a response of opposite signs in the two sets of perturbation experiments can be regarded as robust. This can be quantified by taking the difference (Eq. A.9) and sum (Eq. A.10) of the responses in the two directions (see Supplement for details). As seen in Fig. 3.4, the responses are robust in most cases. The exceptions are $O_{2,eq}$ and $O_{2,dis,bio}$ in the circulation experiment, and $O_{2,dis,phy}$ and $O_{2,soft}$ in the "All" experiment. Crucially, in both sets of perturbation experiments, $O_{2,dis,bio}$ is the primary driver of O_2 changes resulting from sea ice and iron fertilization, which supports our conclusion that these processes play a leading role in glacial deoxygenation.

3.5 Implications for estimates of ocean carbon storage during the LGM

The development of quantitative O_2 proxies opens up the powerful possibility of better constraining glacial ocean carbon storage using the Apparent Oxygen Utilization (AOU) method, the most widely used approach for estimating the inventory

of respired carbon in the ocean. AOU is the difference between the saturation concentration $O_{2,sat}$ of O_2 in a water sample (estimated from its temperature and salinity) and its *in situ* concentration. Assuming that the water was in solubility equilibrium when it was last at the surface of the ocean, this difference is typically attributed to O_2 consumed during soft-tissue regeneration (C_{soft}) as the water is transported from the surface into the interior [23]. Observed higher levels of AOU in the deep ocean during the LGM relative to present day have been used to conclude that the ocean contained more C_{soft} during the glacial period, leading to a drawdown in atmospheric CO_2 [7, 58, 61, 65]. Air-sea disequilibrium complicates this straightforward interpretation of AOU in two ways.

First, O_2 disequilibrium, shown here to be greater during the LGM, violates a key assumption of the AOU method. For instance, if surface waters are undersaturated, the true O_2 utilization will be smaller than that predicted by AOU, leading to an overestimate of C_{soft} [20, 25, 26, 79] (by as much as 50% in the global inventory according to a recent study [20]). Second, it has long been recognized that disequilibrium of CO_2 amplifies the direct effect of C_{soft} on ocean carbon storage [77]. This biologically-mediated component of DIC, $C_{dis,bio}$, has been shown to be also much larger during the LGM [20, 41]. It is therefore more appropriate to define total biological carbon storage, C_{bio}, as a sum of C_{soft} and $C_{dis,bio}$. While both aspects have been acknowledged as a source of uncertainty in AOU-based estimates of glacial biological carbon storage, it has been argued that, if anything, in the presence of disequilibrium AOU systematically underestimates C_{bio} [7, 58]. Here, we combine our O_2 decomposition with a previous carbon one [20] to show that the extent to which proxy-based estimates of AOU capture true glacial biological carbon storage depends sensitively on the mechanisms involved.

The change in biological carbon storage is estimated from AOU according to: $\Delta C_{bio}(AOU) = R_{C:-O_2} \times \Delta AOU$, where $R_{C:-O_2}$ is a constant carbon-to-oxygen stoichiometric ratio. ΔAOU can be expressed in terms of its components as (see Supplement):

$$\Delta AOU \approx -\Delta O_{2,soft} - \Delta O_{2,dis,bio} - \Delta O_{2,dis,phy}, \tag{3.2}$$

demonstrating the explicit dependence of $\Delta C_{bio}(AOU)$ on the disequilibrium components.

Fig. 3.5 shows how the cumulative sum of the O_2 terms in Eq. 3.2 is related to that of the corresponding carbon components, ΔC_{soft}, $\Delta C_{dis,bio}$ and $\Delta C_{dis,phy}$, respectively, for the various perturbation experiments. (For the relationship between the individual components see Fig. A.25 and for reverse perturbation experiment with PIC on the LGM configuration see Fig. A.26.) By construction, ΔC_{soft} and $\Delta O_{2,soft}$, which are both diagnosed from the regenerated phosphate concentration, are exactly proportional to each other via the Redfield (stoichiometric) ratio $-R_{C:-O_2}$ (shown by the dashed grey line). When the biological disequilibrium term is added, this relationship remains strong for the "purely" biological iron fertilization and SI-bio experiments because $\Delta C_{dis,bio}$ and $\Delta O_{2,dis,bio}$ roughly follow the Redfield line (Fig. A.25). The latter relationship becomes weaker in SI-gasx, causing $\Delta C_{soft} + \Delta C_{dis,bio}$ to deviate from the expected Redfied relationship with $\Delta O_{2,soft} + \Delta O_{2,dis,bio}$. (The full sea ice experiment is intermediate between SI-gasx and SI-bio.) In the circulation experiment, $\Delta C_{dis,bio}$ and $\Delta O_{2,dis,bio}$ are almost orthogonal to the Redfield line, causing a large deviation from the Redfield estimate of AOU change and deep carbon change. (The changes in $O_{2,dis,bio}$ and $C_{dis,bio}$ in the temperature experiment are too small to discern a systematic pattern.) The "All" experiment, which can be regarded as a sum of the iron fertilization, sea ice and circulation experiments, also falls close to the Redfield line.

ΔAOU also contains a physical disequilibrium component, $\Delta O_{2,dis,phy}$, which can impact its relationship with ΔC_{bio}. In particular, in the sea ice experiment, which shows the largest effect on O_2 of any single parameter examined, both $O_{2,dis,bio}$ and $O_{2,dis,phy}$ are enhanced (become more negative) leading to a large decrease in deep ocean oxygen, despite reduced consumption. On the other hand, sea ice has a much smaller effect on glacial carbon storage because physical air-sea disequilibrium serves to decrease DIC, whereas biologically-mediated disequilibrium serves to increase DIC by preventing outgassing of carbon-rich upwelled waters, such that there is a cancellation of much of the effect of sea ice on CO_2 air-sea gas

exchange [20]. This ultimately breaks down the relationship between AOU and biological carbon storage, such that AOU overestimates the change in biological carbon storage by over a factor of three (ΔC_{bio}=99 PgC; ΔC_{bio} (AOU)=334 PgC) in this experiment. A similar overestimation is found in the circulation experiment (ΔC_{bio}=−102 PgC; ΔC_{bio} (AOU)=−253 PgC).

Interestingly, in the "All" experiment ΔAOU appears to be a good proxy for ΔC_{bio}. But we note that this is because the change in $C_{dis,phy}$ is quite small due to compensating effects from circulation, temperature and sea ice [20]. We believe that while the effect of different processes on individual O_2 and carbon components in our model is qualitatively quite robust, quantitative changes in those components and their interactions are likely to be model- and state-dependent. Such a cancellation, and hence the ability of AOU to quantify changes in C_{bio}, is therefore unlikely to be robust.

To summarize, the simulated deep ocean deoxygenation in the LGM is consistent with proxy data. O_2 concentrations decrease despite a reduction in modeled export production in the glacial ocean, which leads to a reduction in respired carbon (and thus O_2 consumption), i.e., a less efficient biological carbon pump as conventionally defined. Previous studies [13, 57] have instead interpreted the same proxy-based evidence of glacial deoxygenation as implying an increase in the efficiency of the soft-tissue pump. We find instead that greater air-sea O_2 disequilibrium during the LGM, caused by an expansion in sea ice cover in the Southern Ocean, along with greater iron fertilization, provides a better explanation for lower O_2 concentrations in the glacial deep ocean.

Our results also suggest that the observed increase in AOU in the LGM was primarily caused by biologically-mediated disequilibrium, compounded by physical disequilibrium. The latter can decouple AOU from biological carbon storage, implying that caution must be exercised in interpreting quantitative O_2 proxies in terms of carbon storage.

Our model likely does not capture the complex nature of gas exchange in regions such as the Southern Ocean, where it may be altered by, for example, the

presence of leads in sea ice and seasonal polynyas [63, 79, 108]. To refine our understanding of glacial–interglacial changes in ocean carbon and O_2 distributions, more extensive seasonal observations of O_2 gas exchange, especially in the Southern Ocean, are required. The magnitude of disequilibrium should also be investigated both in models that do not base respired carbon estimates on AOU and that incorporate recent developments in using flexible stoichiometry [110, 111]. The results of recent studies with such models suggest that this may enhance glacial C_{bio} storage [73, 111] and may slightly reduce the quota of O_2 required to respire C_{soft} [111], which could alleviate deoxygenation.

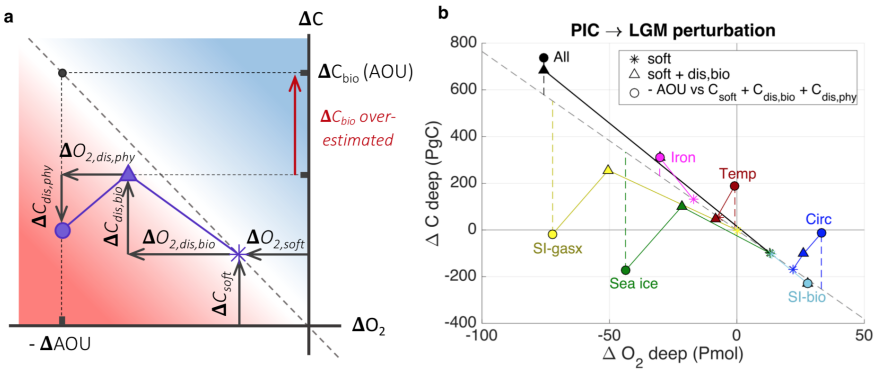

Figure 3.5: Relationship between ΔO_2, ΔAOU and biological carbon storage. a) Schematic showing how use of AOU can lead to over- or underestimation of biological carbon storage. For a given ΔC_{bio} ($= \Delta C_{soft} + \Delta C_{dis,bio}$), the ratio of carbon to O_2 disequilibrium relative to the (negative of) Redfield C:$-O_2$ ratio (dashed grey line) controls whether AOU under- or over-estimates the change in true biological carbon storage. In a plot of ΔAOU versus ΔC_{bio}, for points that plot in the red (blue) region below (above) the Redfield line, ΔC_{bio}(AOU) over- (under-) estimates ΔC_{bio}. Only for points that fall on the line does ΔC_{bio}(AOU) accurately quantify biological carbon storage change. Physical disequilibrium can cause further deviation from the Redfield line which affects ΔAOU. b) ΔO_2 versus ΔC in the deep ocean (below 1000 m) for the perturbation experiments where an LGM condition is imposed on the preindustrial configuration. Changes are shown for the following perturbations: "All" (black); sea ice (green) which is further separated into the gas exchange effect (SI-gasx, yellow), and biological light limitation effect (SI-bio, light blue); iron fertilization (pink); temperature (red); and circulation (dark blue). For each perturbation three components of the carbon-oxygen system are shown: soft-tissue components ($\Delta O_{2,soft}$ and ΔC_{soft}) (stars); soft-tissue and biological disequilibrium components ($\Delta O_{2,soft} + \Delta O_{2,dis,bio}$ and ΔC_{bio}) (triangles); total O_2 and C change from soft-tissue, biological and physical disequilibrium (ΔAOU and $\Delta C_{bio} + \Delta C_{dis,phy}$).

3.6 Methods

The model set up used for this study is described in [20] and references therein. Briefly, the biogeochemical model used is the Model of Ocean Biogeochemistry and Isotopes (MOBI), which has the limiting nutrients dissolved nitrogen, phosphorus and iron, two phytoplankton functional groups, one zooplankton class, dissolved and particulate organic matter and dissolved inorganic carbon (DIC), O_2 and alkalinity [22]. All components of the model track carbon and nitrogen isotopes. The interactive iron cycle is driven externally from atmospheric dust, sediments and hydrothermal vent inputs [89]. Monthly climatologies of atmospheric soluble iron fluxes are used that were generated using monthly dust flux climatologies of both preindustrial control (PIC) and Last Glacial Maximum (LGM) [88], using a constant iron dust content of 3.5% [112] and using a fitted function of iron flux and iron solubility [89]. The dust flux climatologies were constructed by interpolation of Holocene and glacial dust flux data from terrestrial and marine sediments, and ice cores, primarily from the DIRTMAP 3 database [88]. In the Southern Ocean south of 35°S, the LGM soluble iron flux is multiplied by 10, placing the estimate in line with Antarctic ice cores [49] and marine sediment cores [38] and resulting in a substantially better fit [80] between simulated and observed δ^{15}N and glacial-interglacial export production changes (Fig. A.3). Sedimentary release of dissolved iron is proportional to the flux of organic carbon at the ocean bottom [89]; the LGM sub-grid bathymetry used to calculated this is adjusted for the 110 m glacial sea level drop [113]. MOBI is coupled to the Transport Matrix Method (TMM) [90, 91, 96], a framework for computationally efficient offline tracer simulations. To simulate preformed tracers, the instantaneous, annually repeating surface fields of the MOBI-TMM tracers were used as the boundary condition that was advected and diffused into the ocean interior using the TMM. All equilibrium and perturbation tracer simulations were run for 10,000 years to steady-state.

MOBI-TMM is driven by surface winds, circulation, temperature, salinity and sea ice from UVic ESCM (version 2.9) [95], a 3-D ocean general circulation model ($1.8° \times 3.6° \times 19$ layers) coupled to a 1-layer atmospheric energy-moisture balance,

dynamic-thermodynamic sea ice, and land surface models. Preindustrial control (PIC) and Last Glacial Maximum (LGM) simulations used were tuned to a suite of modern biogeochemical and LGM sedimentary isotope (δ^{13}C, $\Delta^{14}C$ and δ^{15}N) records, as previously described [80, 114]. Briefly, forcing on the LGM simulation was done with atmospheric CO_2 and orbital parameters in accord with 19ka BP, addition of a multimodel mean LGM anomaly wind field stress from the Paleoclimate Intercomparison Project Phase 3 (PMIP3) to the present day climatological field, a PMIP3 reconstruction of the continental ice sheet [115], and a global addition of 1-PSU (Practical Salinity Unit) to salinity consistent with glacial sea level drop. The consistency of simulated large-scale tracer distributions with observations have been demonstrated previously for the equilibrium solutions [20, 80]. The characteristics of the model's LGM state are consistent with observational studies, namely, colder global mean temperature (ΔT=-2.5°C compared to -2.6°C from ice core noble gas measurements [116]) and patterns of sea surface temperature change [47, 48]; a weaker and shallower Atlantic Meridional Circulation (AMOC) (as implied by the δ^{13}C distribution and ∼600 year-older $\Delta^{14}C$ deep ocean ages [15, 82]); extended sea-ice extent [107]; and enhanced surface iron fluxes to the Southern Ocean (required to reproduce observed δ^{13}C [80] and δ^{15}N data).

Chapter 4

Conclusions and Future Work

The work in this thesis details the first full O_2 decomposition model applied to the preindustrial and LGM ocean. Simulations were run in these two climate configurations using a coupled ocean biogeochemical model so that the effect of O_2 disequilibrium could be accurately quantified, and the effect of O_2 disequilibrium on AOU-based estimates of carbon storage could also be calculated. Using the Transport Matrix Method allowed for the biogeochemical model to be run offline with these additional preformed O_2 tracers. Perturbation experiments were conducted to assess the effect of LGM conditions on the distribution of O_2 and the decomposed components. Given the previous work conducted using the UVic-MOBI2.0 model for a full carbon decomposition analysis of the preindustrial and LGM oceans, including perturbation experiments [20], differences and similarities in the response of CO_2 and O_2 were identified for both climate states. The effect of physically- and biologically-mediated O_2 disequilibrium on the magnitude of AOU were also analysed for perturbation experiments, with the qualitative effects on biological carbon storage estimates discussed.

The modelled preindustrial ocean had a larger O_2 content than the LGM ocean, consistent with O_2 proxy data showing deep ocean deoxygenation. The preindustrial ocean simulation showed surface disequilibrium similar to data from floats. Present day surface waters are often in a state of disequilibrium, particularly negative disequilibrium at high latitudes near regions of bottom and intermediate water formation. Seasonal differences in the pattern of surface under- and over-saturation

occur regionally with phytoplankton blooms releasing O_2, and wintertime mixed layer deepening and cooling driving undersaturation. Surface undersaturation was most pronounced in the Southern Ocean in both the preindustrial and LGM simulations. The magnitude of undersaturation caused by biological disequilibrium was greater in the LGM than the preindustrial simulations and was the major contributor to the decline in the total O_2 content of the LGM ocean. Despite the cooler temperature increasing O_2 solubility in the LGM, the effects of more extensive sea ice and Southern Ocean iron fertilisation, in particular, drove this negative biological disequilibrium. These worked in a synergistic manner to create a very large negative biological disequilibrium greater than the sum of the individual effects seen in the individual perturbation experiments, demonstrating nonlinearity of the system.

The major driver of LGM deoxygenation, namely sea ice, did not have a significant effect on enhancing glacial ocean carbon storage. This was because sea ice prevented outgassing of upwelled carbon-rich waters (positive biological disequilibrium) but also prevented in-gassing expected due to cooling of poleward moving waters (negative physical disequilibrium). These effects largely cancelled out in the case of carbon, such that sea ice was determined to be a minor contributor to changes in glacial ocean carbon storage. In O_2 sea ice perturbation experiments, both the physical disequilibrium effect and the biologically-mediated disequilibrium were negative as upwelled waters were instead O_2 poor. This cumulative effect, combined with a net increase in productivity when iron fertilisation occurred in the experiment with all perturbations, accounted for the large drop in deep ocean O_2 in the glacial simulation. This is consistent with proxy data.

The effect of negative O_2 disequilibrium was to make AOU larger, as these contributed to O_2 depletion in addition to the effect of aerobic respiration. The effect of individual perturbations were not additive when all were then implemented, demonstrating these effects on the carbon and O_2 systems are nonlinear and likely model and state specific. AOU-based estimates of carbon storage deviated from the true figures due to this nonlinear response of the O_2 system to different glacial boundary conditions, and the disconnect between the O_2 and carbon disequilibrium

brought about by different reactions to physical versus biological changes. Until a particular model has been analysed for the effect of O_2 disequilibrium on AOU, estimates of carbon storage may carry significant errors.

The large, negative O_2 disequilibrium seen in the glacial simulation was similar to those found by Eggleston and Galbraith [79]. They traced total disequilibrium O_2 in a glacial-type configuration using a coupled general circulation-biogeochemical ocean model of similar complexity to the UVic-MOBI2.0 model. However, by further differentiating between the physical and biological O_2 disequilibrium, I have demonstrated the nonlinearity of the O_2 system and the reason for similarities and differences between carbon disequilibrium and O_2 disequilibrium. This is important given most of the perturbation experiments demonstrated both physical air-sea gas exchange disequilibrium effects as well as changes to the biological consumption of O_2 and therefore the biologically-mediated O_2 disequilibrium. Eggleston and Galbraith observed that there was mostly an anti-correlation between carbon and O_2 disequilibrium; the differentiation between physical and biological disequilibrium for both carbon and O_2 explains this as solubility driven changes effect CO_2 and O_2 in the same direction with magnitude effected by differences in solubility properties. On the other hand, biologically-mediated disequilibrium effects CO_2 and O_2 in opposing directions and in a stoichiometry determined by phytoplankton nutrient usage.

The research presented in this thesis showed that sea ice was particularly important for LGM deep ocean deoxygenation through enhancing the negative biological disequilibrium. Sea ice was modelled using a dynamic-thermodynamic model [95] but did not include the effect of leads, which are cracks in the ice that can allow for air-sea gas exchange. Another phenomenon not considered were polynyas, which are large areas of open water in the sea ice [117]. Both leads and polynyas allow for more air-sea gas exchange, which can reduce negative disequilibrium, and can allow for more phytoplankton growth in the spring and summer, as well as changes to the rate of Antarctic Bottom Water (AABW) formation and global circulation [118]. Parameterisations for incorporating polynyas into general circulation models (GCMs) exist for the modern ocean [118, 119] but are not yet widely incorporated

into coupled GCM-biogeochemical models and have not been developed for the glacial ocean. Fossil records of foraminifera indicate the presence of seasonal and perennial polynyas in the glacial Weddell Sea [108], an important region near Antarctica where AABW forms. Should polynyas be included in preindustrial and glacial models, the results found in this study would likely provide an upper limit for the effect of sea ice on glacial O_2 disequilibrium. The incorporation of polynyas and leads into glacial and preindustrial ocean models would allow for exploration of their effect on both the O_2 and CO_2 content of the AABW that forms near these regions, and the global ocean O_2 and carbon budgets. Including leads and polynyas in future models would a valuable experiment.

Another area of research that would be valuable to include in future studies is the incorporation of variable Redfield stoichiometry. This was not included in this research as it had not been developed for the MOBI2.0 model at the time of this study. Based on the results of the variable stoichiometry glacial ocean model presented by Ödalen [73], if an increase in the carbon:phosphorus ratio occurs, this would result in a further depletion of O_2 relative to a fixed stoichiometry scenario. However, the glacial boundary conditions applied in their model are significantly different from the UVic-MOBI2.0 model. They also used an AOU-based method to calculate carbon storage changes so true results for changes in carbon storage and biological pump may not be similar to the MOBI2.0 model. The effect of disequilibrium in particular would require modelling in case of counterintuitive changes in the carbon system, O_2 system, or both.

Previous modelling studies of the glacial ocean have not taken O_2 disequilibrium into account. The results of this work indicate that these previous AOU-based estimates of glacial ocean carbon storage may carry errors that should be reviewed. This work also provides evidence that caution should be applied when using O_2 proxy data for estimating glacial ocean carbon storage because of the effect of O_2 disequilibrium.

Appendices

Appendix A

Additional Figures and Analyses

Contents

A.1 Decomposition of O_2

Here, a more comprehensive explanation of the decomposition of O_2 is provided. To track O_2 through the model, total O_2 is expressed as the sum of preformed O_2 ($O_{2,\mathrm{pre}}$) and O_2 consumed from the respiration of soft-tissue ($O_{2,\mathrm{soft}}$) (Eq. A.1).

$$O_2 = O_{2,\mathrm{pre}} + O_{2,\mathrm{soft}} \tag{A.1}$$

A preformed tracer is a conservative tracer whose value is set at the surface of the ocean and is passively transported into the interior by the circulation. $O_{2,\mathrm{soft}}$ is negative as respiration removes O_2, whereas respired carbon (C_{soft}) is positive as it

is released when soft-tissue is regenerated. $O_{2,\text{soft}}$ and C_{soft} are calculated as:

$$O_{2,\text{soft}} = (-1/R_{C:-O_2}) \times C_{\text{soft}} \quad (A.2)$$

$$C_{\text{soft}} = R_{C:P} \times PO_{4,\text{reg}} \quad (A.3)$$

$$PO_{4,\text{reg}} = PO_4 - PO_{4,\text{pre}}, \quad (A.4)$$

where we relate $O_{2,\text{soft}}$, C_{soft} and regenerated phosphate ($PO_{4,\text{reg}}$) via a fixed Redfield stoichiometry for C:P:O_2. The phosphate inventory is fixed in the ocean model, and to calculate $PO_{4,\text{reg}}$ we simulate a preformed phosphate ($PO_{4,\text{pre}}$) tracer for each experiment by propagating the seasonally-varying surface ocean phosphate field into the interior using the TMM. The difference between PO_4 and $PO_{4,\text{pre}}$ at the end of each run is the regenerated phosphate (Eq. A.4).

To simulate $O_{2,\text{pre}}$ we similarly propagate the seasonally-varying surface ocean O_2 field into the interior. $O_{2,\text{pre}}$ is further decomposed into equilibrium and disequilibrium components by simulating an additional tracer, $O_{2,\text{eq}}$, by propagating the surface theoretical equilibrium O_2 into the interior. $O_{2,\text{pre}}$ and $O_{2,\text{eq}}$ are simulated for each experiment. The disequilibrium component $O_{2,\text{dis}}$ of preformed O_2 is then calculated by taking the difference between $O_{2,\text{pre}}$ and $O_{2,\text{eq}}$:

$$O_{2,\text{dis}} = O_{2,\text{pre}} - O_{2,\text{eq}} \quad (A.5)$$

Waters may be oversaturated at the surface ($O_{2,\text{pre}} > O_{2,\text{eq}}$ so $O_{2,\text{dis}} > 0$) or undersaturated ($O_{2,\text{pre}} < O_{2,\text{eq}}$ so $O_{2,\text{dis}} < 0$).

The O_2 decomposition in Eq. A.1 is more completely described by:

$$O_2 = \underbrace{O_{2,\text{eq}} + O_{2,\text{dis,phy}} + O_{2,\text{dis,bio}}}_{O_{2,\text{pre}}} + \underbrace{(-R_{-O_2:P}) \times PO_{4,\text{reg}}}_{O_{2,\text{soft}}} \quad (A.6)$$

For every experiment the full physical-biogeochemical model is run to steady state. We also run a parallel simulation where the physical forcings (circulation, temperature, salinity, winds, etc) are the same, but the source/sink terms in the biogeochemical model are switched off. Nutrients, DIC and O_2 are all transported by the TMM but do not get used in biological processes. As such, this parallel

simulation gives us a reference point for the ocean without any biological activity. $O_{2,eq}$, which only depends on temperature and salinity, is identical in the full physical-biogeochemical simulation and physics-only simulation. The disequilibrium component of preformed O_2 in the physics-only experiment, $O_{2,pre,phy}$, is then purely a result of physical processes (e.g., temperature gradients, sea ice blocking gas exchange) for the conditions of that simulation (Eq. A.7). In the parallel full physical-biogeochemical simulations, biological processes will change the distribution of DIC and O_2, and thus change O_2 disequilibrium. We attribute any difference in disequilibrium between the full and physics-only experiments to biological processes (Eq. A.8).

$$O_{2,dis,phy} = O_{2,pre,phy} - O_{2,eq} \tag{A.7}$$

$$O_{2,dis,bio} = O_{2,dis} - O_{2,dis,phy} \tag{A.8}$$

This procedure of running parallel sets of physics-only and full simulations is carried out for the PIC and LGM equilibrium experiments, as well as all perturbation experiments. In the physics-only simulations for the perturbation experiments the model starts from the steady state of the corresponding physics-only base run (e.g., PIC for PIC→LGM perturbations), while for the full physical-biogeochemical perturbation simulations the model starts from the steady state of the corresponding full physical-biogeochemical base run. The perturbations applied is the same in both cases. At the end of each perturbation run, the decomposition is performed as explained above and differences from the respective base states give us the perturbation effect on each O_2 component.

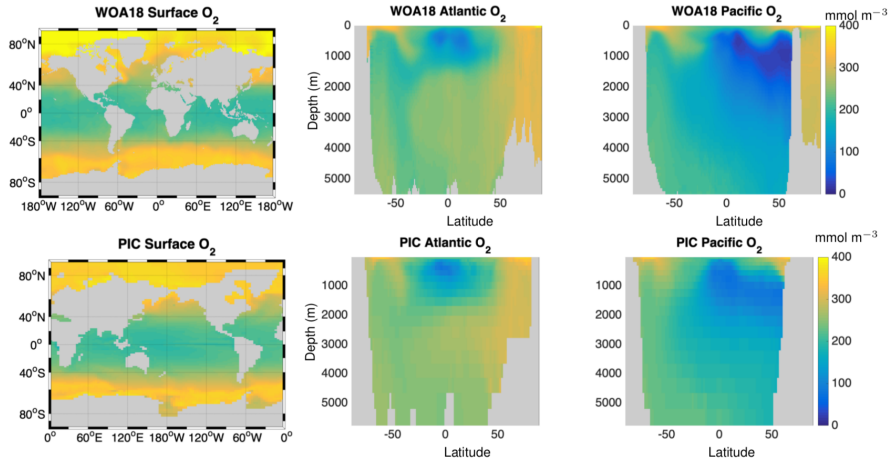

Figure A.1: Annual mean O_2 in World Ocean Atlas 2018 (WOA18) and the preindustrial control (PIC) simulation. Top row: surface, Atlantic and Pacific zonal mean sections of WOA18 O_2. Bottom row: PIC surface, Atlantic and Pacific zonal mean sections of O_2.

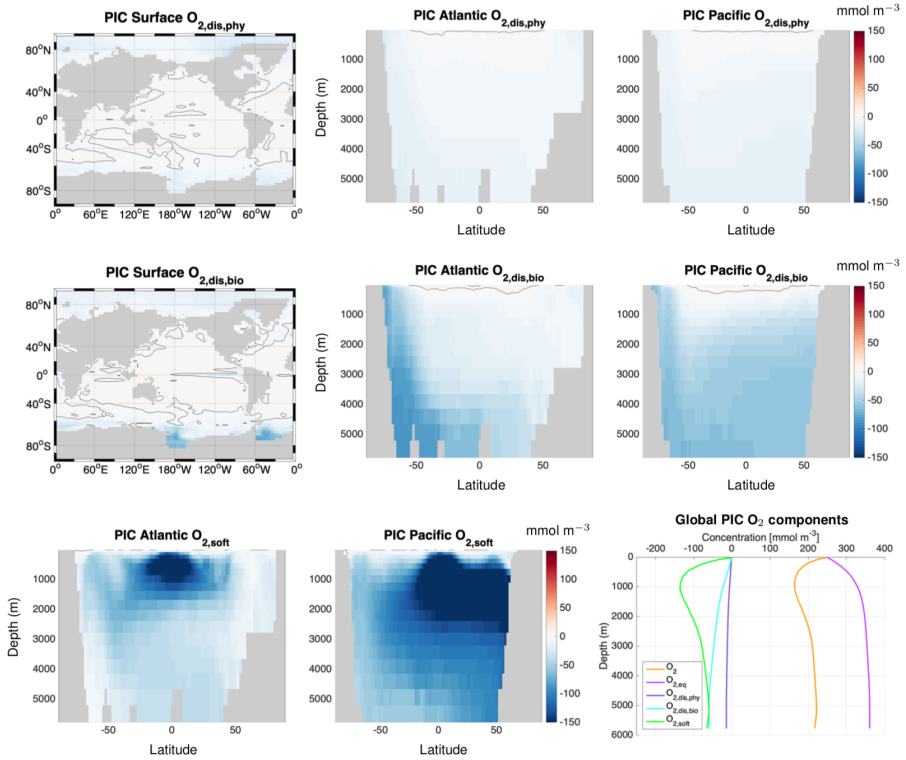

Figure A.2: Oxygen decomposition for the PIC equilibrium simulation. Top row: surface, Atlantic and Pacific zonal mean meridional sections of $O_{2,\mathrm{dis,phy}}$. Middle row: surface, and Atlantic and Pacific zonal mean meridional sections of $O_{2,\mathrm{dis,bio}}$. Bottom row: Atlantic and Pacific zonal mean meridional section of $O_{2,\mathrm{soft}}$, and (left) global horizontal average of O_2 (orange), $O_{2,\mathrm{eq}}$ (pink), $O_{2,\mathrm{dis,phy}}$ (purple), $O_{2,\mathrm{dis,bio}}$ (blue) and $O_{2,\mathrm{soft}}$ (green); Black solid line is the zero contour.

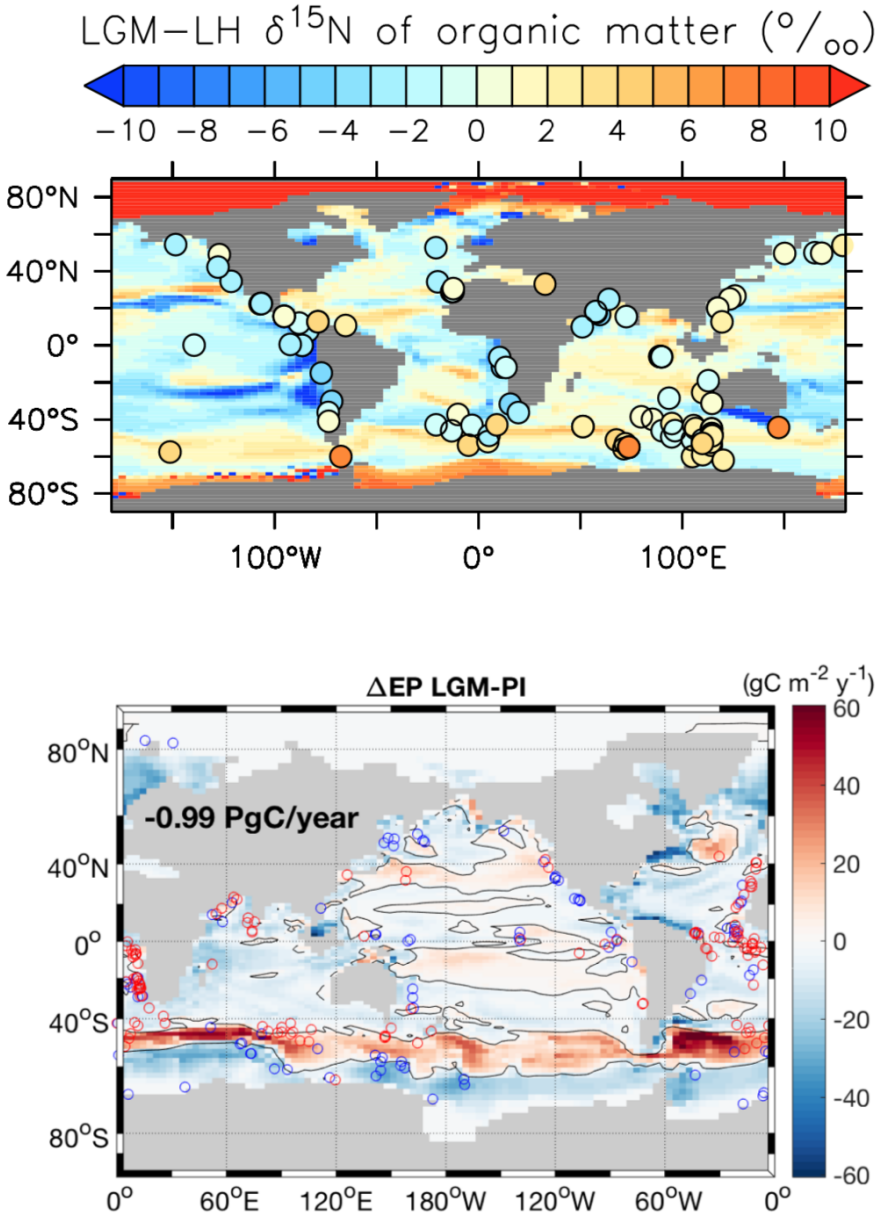

Figure A.3: Changes in nitrogen isotopes and export production (EP) between the LGM and PIC. This figure is reproduced from [20] for the convenience of the reader. Top: Difference between simulated surface δ^{15}N of detrital (particulate organic) matter in modeled LGM and PIC, averaged over the top 120m of the water column. LGM-PIC values from observations [22, 53, 120] are overlaid. Bottom: Difference between LGM and PIC simulated EP. Zero contour is the black solid line. The pattern of change simulated shows reasonable agreement with proxy-based reconstructions [103] (circles) of the direction of change (red: higher LGM EP; blue: lower LGM EP).

A.2 Distribution of preindustrial control O_2 components

A.3 Comparison of LGM-PIC ΔO_2 and productivity reconstructions with model results

To facilitate comparison of data and model, the nearest ocean model grid point was found and used for comparison with proxy reconstructions of O_2. Qualitative O_2 proxy data indicate whether the change in O_2 concentration between LGM and Holocene was positive, negative or ambiguous [121]. Of a total of 110 qualitative proxy data points available from the literature, 89 showed a clear decrease or increase in LGM O_2, with the remaining being classified as ambiguous. We include in the qualitative data results using the I/Ca content of pelagic foraminifera as the method, while described as “semi-quantitative" [63], is reliant on oxidation thresholds. Comparison of these 89 data values with the model shows an agreement for 55 of them (Table A.1). The model agreement with reconstructions is poorest in the Indian Ocean, and showed some inconsistencies in the Eastern Equatorial Pacific. These regions are near modern Oxygen Minimum Zones, where there are steep gradients in water column O_2 that are not well-resolved in the model, which may account for these inconsistencies.

We have also compared available quantitative proxy data to assess the magnitude of change between the model and reconstructions. Below ∼2000 m deoxygenation is a consistent trend in the model and proxy data. The quantitative data shows strong deoxygenation at all points including those at ∼1400 m (Fig. A.4) and the magnitude of modeled deoxygenation at the same locations. The Eastern Equatorial Pacific (EEP) is the region with the most quantitative proxy records (circles: Fig. A.4). The two data points that show the largest deviation from the model show deoxygenation of ∼140 mmol m^{-3}, which in the EEP data point is a much larger change than reconstructions at nearby sites and is based on a Holocene $\delta^{13}C$ O_2 reconstruction that is over 100 μmol kg^{-1} greater than the *in situ* O_2 concentration measured at the core site [58]. In the South Atlantic, the quantitative reconstruction of LGM

Table A.1: Comparison of qualitative reconstructions and changes in model LGM-PIC O_2: the number of data points that are in agreement or disagreement between the model and proxy reconstructions are shown.

Atlantic basin	Reconstruction		
	Increase	Decrease	Ambiguous
Model Increase	1	1	2
Model Decrease	3	10	0
Pacific basin	**Reconstruction**		
	Increase	Decrease	Ambiguous
Model Increase	18	5	5
Model Decrease	9	14	11
Indian basin	**Reconstruction**		
	Increase	Decrease	Ambiguous
Model Increase	0	2	1
Model Decrease	14	12	2

O_2 depletion is approximately double that in the model ($\sim$-140 mmol m^{-3} versus $\sim$-70 mmol m^{-3}). ΔO_2 is determined relative to the present day O_2 at the site and has an error of $\sim$40 μmol kg^{-1} [66], indicating uncertainty in this reconstruction. As such, while the model does not capture the full magnitude of deoxygenation that has been reconstructed, given variability and uncertainties that remain in the reconstructions, we are confident in the broad-scale changes seen in the model.

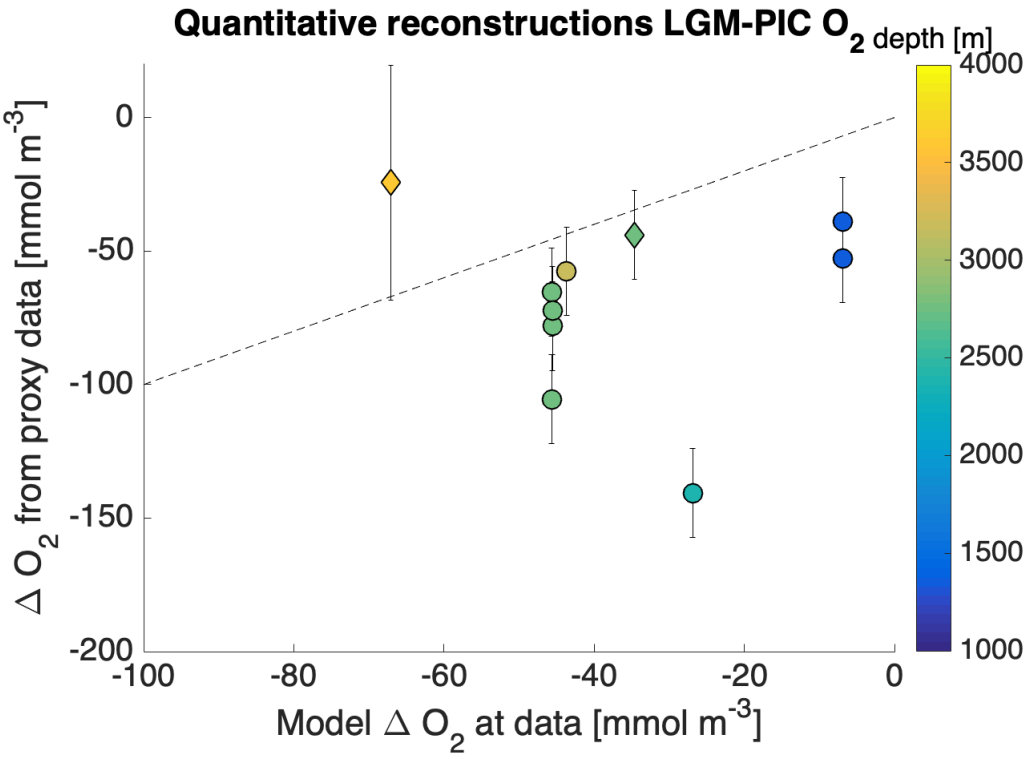

Figure A.4: Comparison of modeled LGM-PIC O_2 difference with quantitative proxy data. Data points are present in the Pacific (circles) and Atlantic (diamonds) basins. The depth of the points are shown as the midpoint of the grid box closest to the data location. Reported standard deviations for the reconstructed values are shown. The dashed line is a one-to-one line.

A.4 Additional plots of LGM-PIC for O_2 components

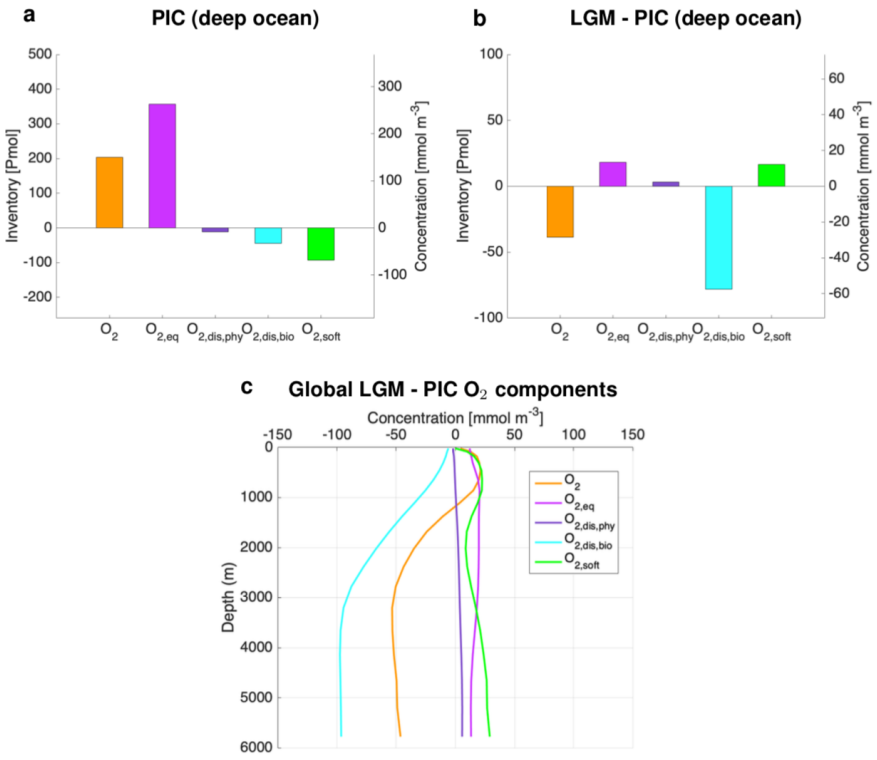

Figure A.5: The components of deep ocean (below 1000 m) O_2 in PIC and LGM relative to PIC. (a) Oxygen decomposition for the PIC equilibrium simulation, and (b) the difference between the LGM and PIC equilibrium simulations shown as inventories in Pmol O_2 (left axis) and concentrations in mmol m^{-3} (right axis). These vary slightly from the whole ocean decomposition (Fig. 3 in main text). (c) Global horizontally-averaged concentrations (mmol m^{-3}) of O_2, $O_{2,eq}$, $O_{2,dis,phy}$, $O_{2,dis,bio}$ and $O_{2,soft}$ for the LGM relative to PIC.

A.5 Further perturbation experiment results

A "reverse" set of perturbation experiments was also run to investigate the effect of perturbing the LGM state with PIC conditions (LGM→PIC). Figs. A.8 and A.9 show the decomposition of O_2 components for these perturbation experiments.

A.5.1 Robustness and linearity of responses to perturbations

To evaluate whether a particular process is "robust" and linear in its effect on any given O_2 component, we take the difference between the two sets of perturbation experiments (PIC→LGM and LGM→PIC) and divide by two (Eq. A.9). A robust process will generate a response of the opposite sign between the two directions; the

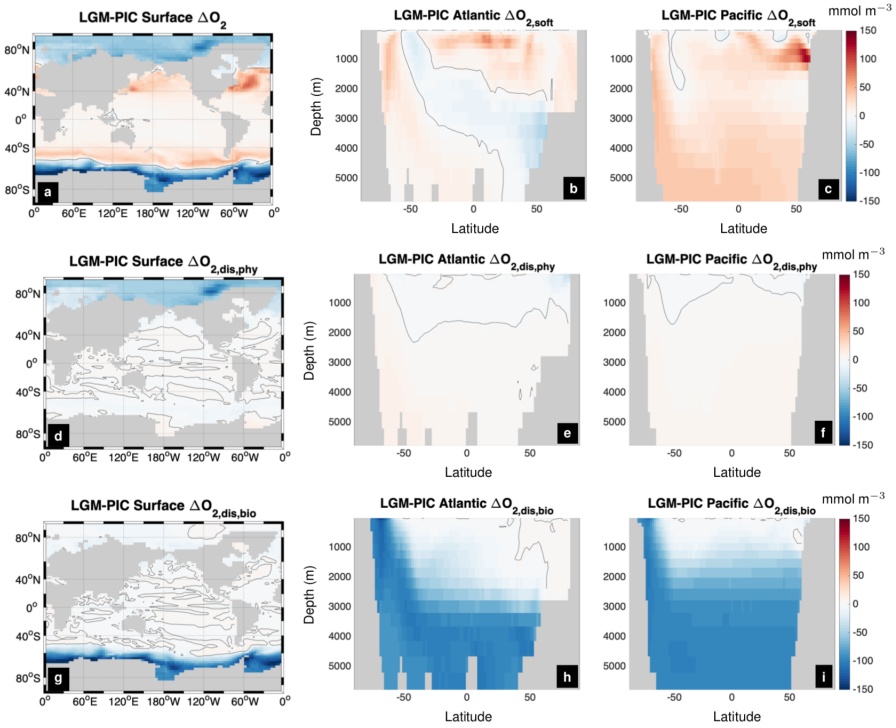

Figure A.6: Oxygen components are shown for the difference between the LGM and PIC equilibrium simulations. (a) surface, Atlantic and Pacific zonal mean meridional sections of LGM-PIC O_2 differences. (b,c) Atlantic and Pacific zonal mean meridional sections of LGM-PIC $O_{2,soft}$ differences. (d-f) surface, Atlantic and Pacific zonal mean meridional sections of LGM-PIC$O_{2,dis,phy}$ differences; (g-i) surface, Atlantic and Pacific zonal mean meridional sections of LGM-PIC $O_{2,dis,bio}$ differences; Black solid line is the zero contour.

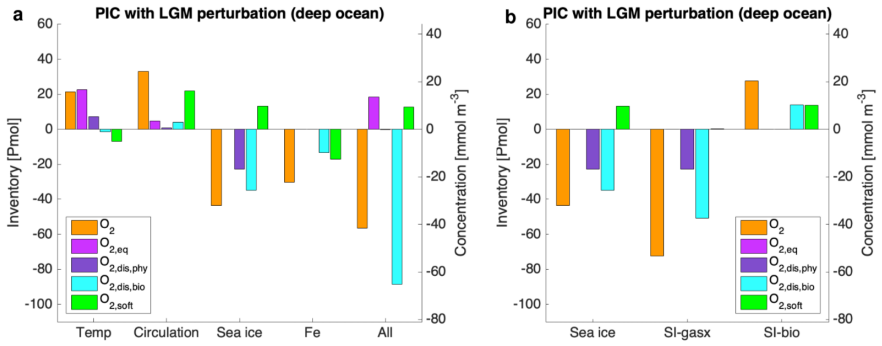

Figure A.7: Response of PIC deep ocean (below 1000 m) O_2 components to LGM perturbations. (a) Change in deep ocean inventory due to a perturbation in circulation; sea ice; temperature; iron; and all perturbations in which LGM temperature, circulation, sea ice, iron fertilization, salinity (1-PSU decrease consistent with 110 m sea level rise) and winds were used to perturb the PIC. (b) Change in deep ocean inventory due to LGM perturbation of sea ice; SI-gasx: effect of sea ice on O_2 gas exchange; SI-bio: sea ice effect on light limitation for biology.

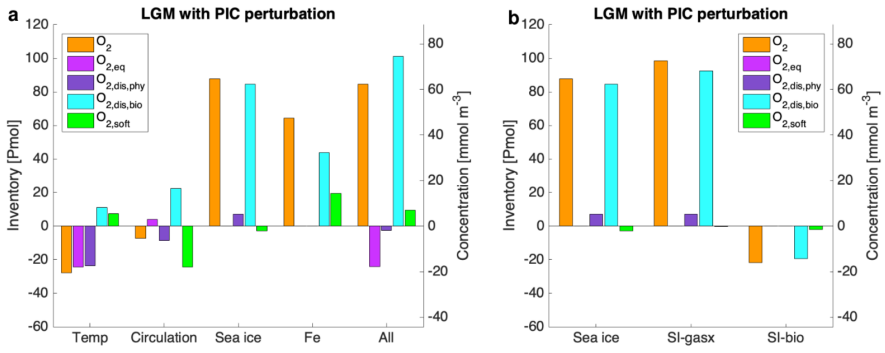

Figure A.8: Response of LGM O_2 components to PIC perturbations. (a) Change in inventory due to a perturbation in circulation; sea ice; temperature; iron; and all perturbations in which PIC temperature, circulation, sea ice, iron fertilization, salinity (1-PSU decrease consistent with 110 m sea level rise) and winds were used to perturb the LGM. (b) Change in inventory due to PIC perturbation of sea ice; SI-gasx: effect of sea ice on O_2 gas exchange; SI-bio: sea ice effect on light limitation for biology.

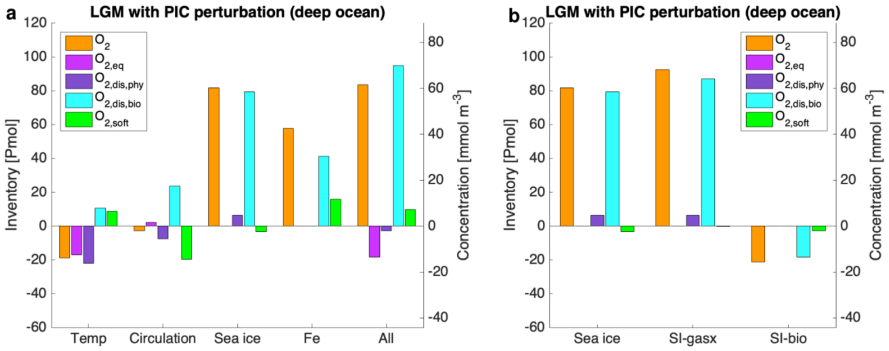

Figure A.9: Response of LGM deep ocean (below 1000 m) O_2 components to PIC perturbations. (a) Change in inventory due to a perturbation in circulation; sea ice; temperature; iron; and all perturbations in which PIC temperature, circulation, sea ice, iron fertilization, salinity (1-PSU decrease consistent with 110 m sea level rise) and winds were used to perturb the LGM. (b) Change in inventory due to PIC perturbation of sea ice; SI-gasx: effect of sea ice on O_2 gas exchange; SI-bio: sea ice effect on light limitation for biology.

difference in response, $\Delta O_{2,x}$(bar), will thus be additive and have a large absolute value. In contrast, a non-robust process will produce the same sign; $\Delta O_{2,x}$(bar) will thus have a small absolute value. To give a sense of how different the responses are in the two directions, the conventional average of the two sets of perturbation experiment sets is taken (Eq. A.10) to give the "range" $\Delta O_{2,x}$(range). If $\Delta O_{2,x}$(bar) has a large absolute value for a given process and O_2 component, and $\Delta O_{2,x}$(range) is relatively small, that indicates a robust and largely linear effect of that process

on that component. On the other hand, if $\Delta O_{2,x}$(range) is greater than $\Delta O_{2,x}$(bar), it suggests a non-robust and nonlinear effect.

$$\Delta O_{2,x}(\text{bar}) = \frac{\Delta O_{2,x}(\text{PIC} \rightarrow \text{LGM}) - \Delta O_{2,x}(\text{LGM} \rightarrow \text{PIC})}{2} \tag{A.9}$$

$$\Delta O_{2,x}(\text{range}) = \frac{\Delta O_{2,x}(\text{PIC} \rightarrow \text{LGM}) + \Delta O_{2,x}(\text{LGM} \rightarrow \text{PIC})}{2} \tag{A.10}$$

Fig. 3.4 shows the results of this exercise. Evidently, the effect of circulation on $O_{2,eq}$ and $O_{2,dis,bio}$ was not robust, although the changes in these components are small to begin with in both directions. Interestingly, $O_{2,soft}$ increased (that is, C_{soft} was reduced) in both "All" experiments, indicating a non-robust and relatively small (10-20 Pmol) change. $O_{2,dis,phy}$ also decreased in the "All" experiment, although the size of the change was very small (< 3 Pmol). The results of the "reverse" perturbation experiments confirms that $O_{2,dis,bio}$ is a key contributor to LGM deep ocean deoxygenation. As seen from the individual perturbation experiments, temperature, iron and sea ice are qualitatively robust processes, supporting the main conclusions of the paper that the combined effects of sea ice and iron fertilization were the primary drivers of the glacial deoxygenation observed in the model. The $O_{2,dis,bio}$ change in the "All" experiment was also extremely robust, although interestingly in each perturbation experiment the change in $O_{2,dis,bio}$ in the LGM to PIC direction was larger than in the PIC to LGM case. This is further evidence for the decoupling that is possible between $O_{2,soft}$ and $O_{2,dis,bio}$, demonstrating how our decomposition allows us to separate and understand the effect of different processes on glacial deoxygenation.

A.5.2 Atlantic and Pacific zonal means of all perturbation experiments

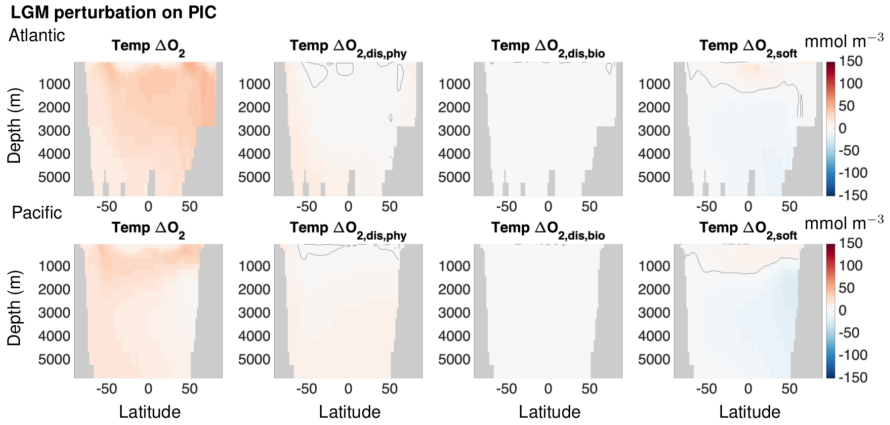

Figure A.10: Zonally-averaged O_2 components in the Atlantic basin (top row) and Pacific basin (bottom row) for the LGM temperature perturbation experiment on the PIC. The O_2, $O_{2,\mathrm{dis,phy}}$, $O_{2,\mathrm{dis,bio}}$ and $O_{2,\mathrm{soft}}$ distributions are shown.

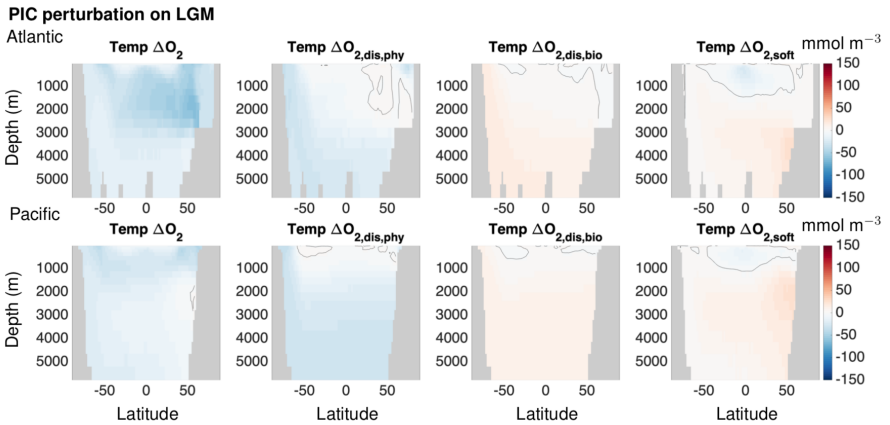

Figure A.11: Zonally-averaged O_2 components in the Atlantic basin (top row) and Pacific basin (bottom row) for the PIC temperature perturbation experiment on the LGM. The O_2, $O_{2,\mathrm{dis,phy}}$, $O_{2,\mathrm{dis,bio}}$ and $O_{2,\mathrm{soft}}$ distributions are shown.

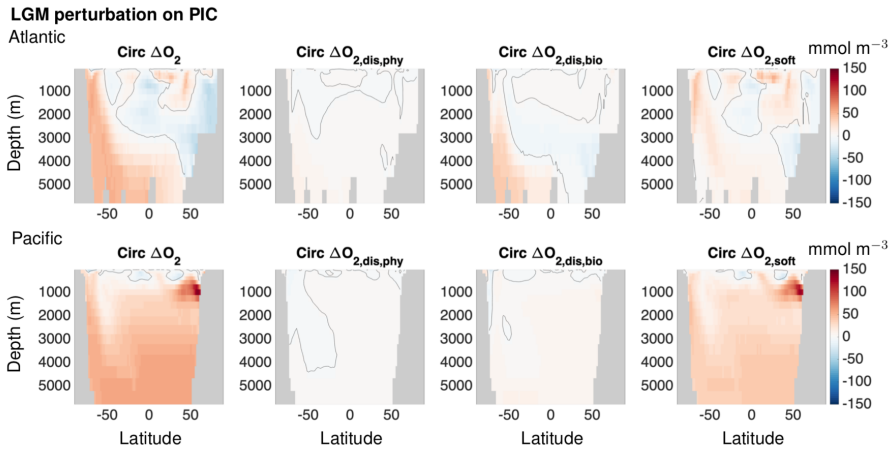

Figure A.12: Zonally-averaged O_2 components in the Atlantic basin (top row) and Pacific basin (bottom row) for the LGM circulation perturbation experiment on the PIC. The O_2, $O_{2,\mathrm{dis,phy}}$, $O_{2,\mathrm{dis,bio}}$ and $O_{2,\mathrm{soft}}$ distributions are shown.

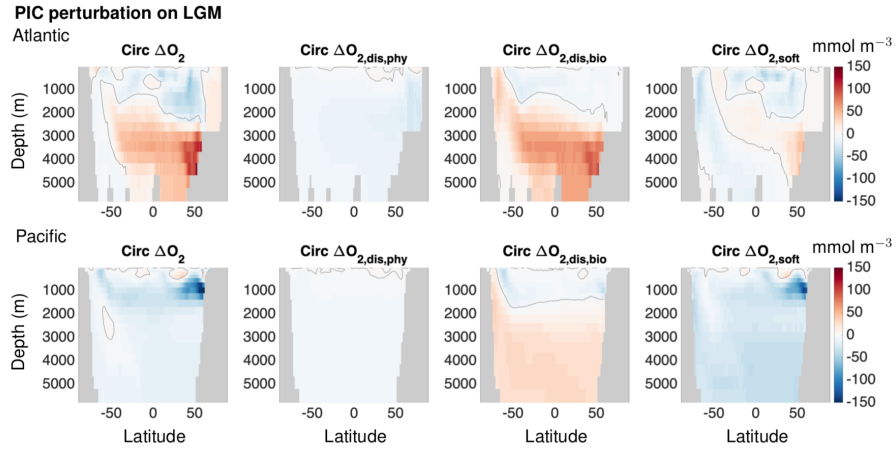

Figure A.13: Zonally-averaged O_2 components in the Atlantic basin (top row) and Pacific basin (bottom row) for the PIC circulation perturbation experiment on the LGM. The O_2, $O_{2,\mathrm{dis,phy}}$, $O_{2,\mathrm{dis,bio}}$ and $O_{2,\mathrm{soft}}$ distributions are shown.

A.6 Decomposition of Apparent Oxygen Utilization (AOU) into O_2 components

We express AOU in terms of its components:

$$\begin{aligned}
\mathrm{AOU} &= \mathrm{O}_{2,\mathrm{sat}} - \mathrm{O}_2 \\
&= \mathrm{O}_{2,\mathrm{sat}} - \left[\mathrm{O}_{2,\mathrm{eq}} + \mathrm{O}_{2,\mathrm{soft}} + \mathrm{O}_{2,\mathrm{dis,bio}} + \mathrm{O}_{2,\mathrm{dis,phy}}\right] \\
&\approx \mathrm{O}_{2,\mathrm{sat}} - \left[\mathrm{O}_{2,\mathrm{sat}} + \mathrm{O}_{2,\mathrm{soft}} + \mathrm{O}_{2,\mathrm{dis,bio}} + \mathrm{O}_{2,\mathrm{dis,phy}}\right] \\
&= -\left[\mathrm{O}_{2,\mathrm{soft}} + \mathrm{O}_{2,\mathrm{dis,bio}} + \mathrm{O}_{2,\mathrm{dis,phy}}\right],
\end{aligned}$$

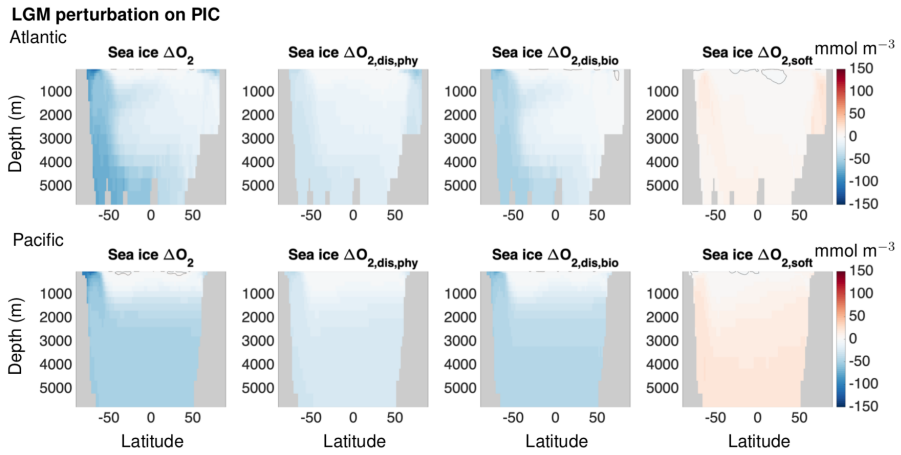

Figure A.14: Zonally-averaged O_2 components in the Atlantic basin (top row) and Pacific basin (bottom row) for the LGM sea ice perturbation experiment on the PIC. The O_2, $O_{2,\mathrm{dis,phy}}$, $O_{2,\mathrm{dis,bio}}$ and $O_{2,\mathrm{soft}}$ distributions are shown.

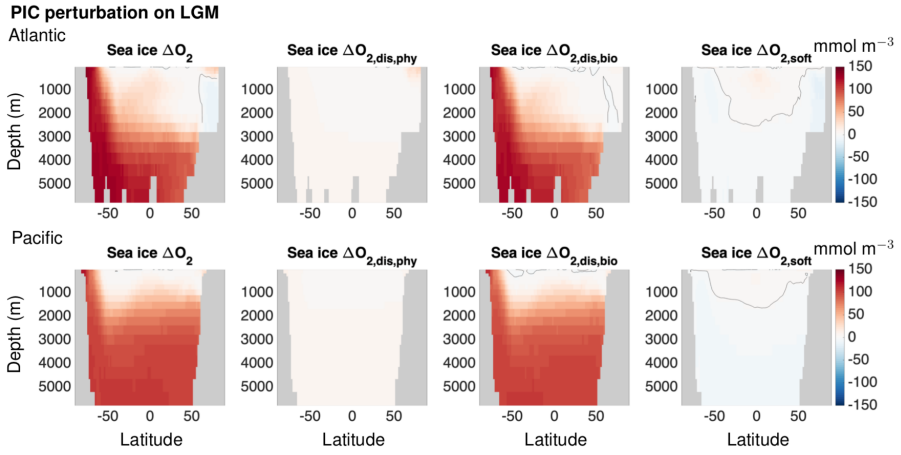

Figure A.15: Zonally-averaged O_2 components in the Atlantic basin (top row) and Pacific basin (bottom row) for the PIC sea ice perturbation experiment on the LGM. The O_2, $O_{2,\mathrm{dis,phy}}$, $O_{2,\mathrm{dis,bio}}$ and $O_{2,\mathrm{soft}}$ distributions are shown.

where we have approximated $O_{2,\mathrm{eq}}$ by $O_{2,\mathrm{sat}}$. Thus, a change in AOU can be written as:

$$\Delta\mathrm{AOU} \approx -\Delta O_{2,\mathrm{soft}} - \Delta O_{2,\mathrm{dis,bio}} - \Delta O_{2,\mathrm{dis,phy}}.$$

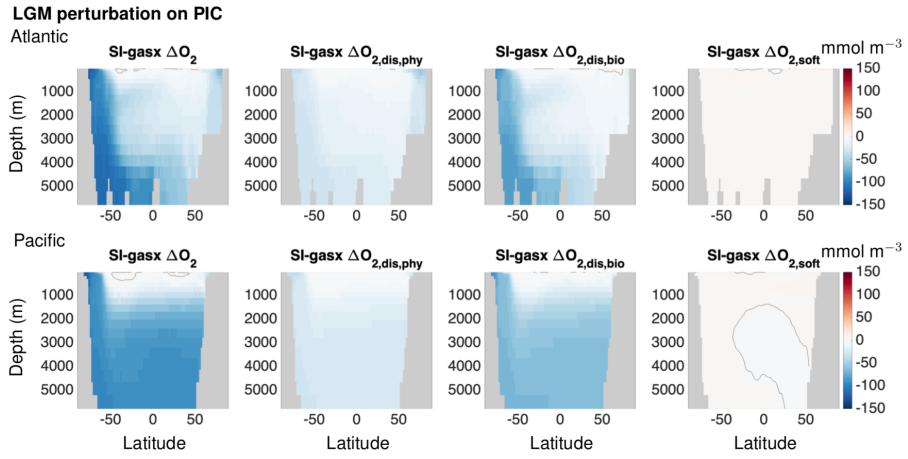

Figure A.16: Zonally-averaged O_2 components in the Atlantic basin (top row) and Pacific basin (bottom row) for the LGM sea ice gas exchange perturbation experiment on the PIC. The O_2, $O_{2,\mathrm{dis,phy}}$, $O_{2,\mathrm{dis,bio}}$ and $O_{2,\mathrm{soft}}$ distributions are shown.

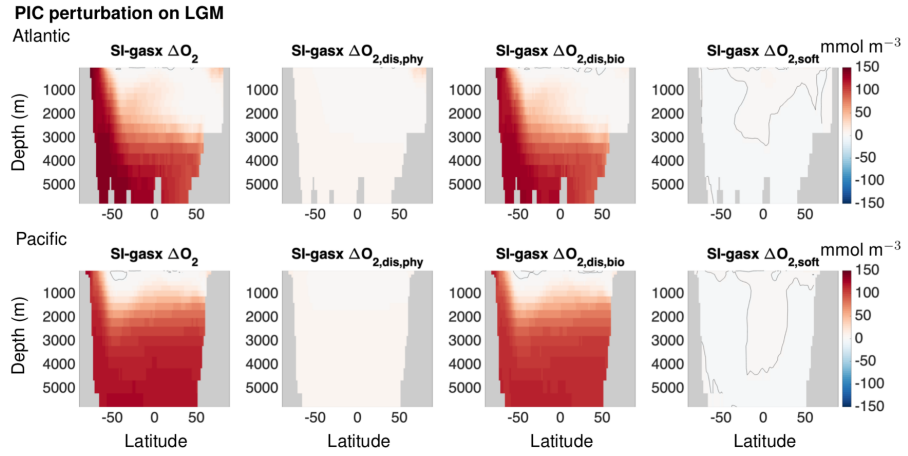

Figure A.17: Zonally-averaged O_2 components in the Atlantic basin (top row) and Pacific basin (bottom row) for the PIC sea ice gas exchange perturbation experiment on the LGM. The O_2, $O_{2,\mathrm{dis,phy}}$, $O_{2,\mathrm{dis,bio}}$ and $O_{2,\mathrm{soft}}$ distributions are shown.

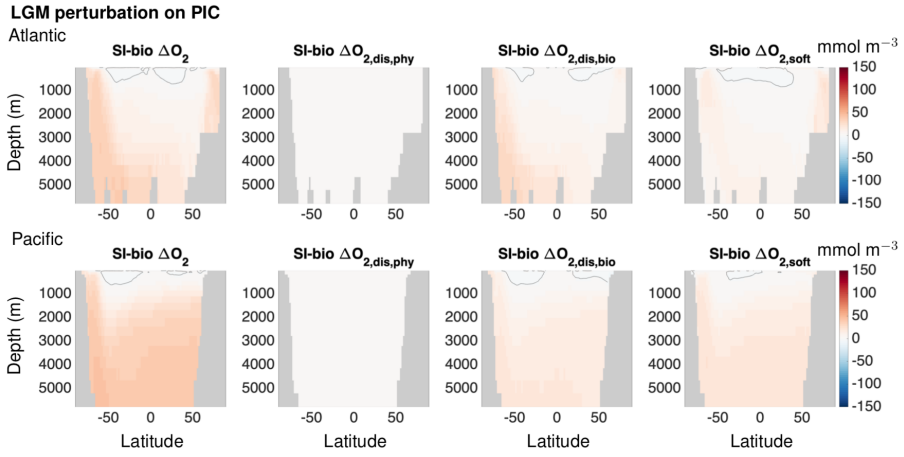

Figure A.18: Zonally-averaged O_2 components in the Atlantic basin (top row) and Pacific basin (bottom row) for the LGM sea ice light limitation perturbation experiment on the PIC. The O_2, $O_{2,\mathrm{dis,phy}}$, $O_{2,\mathrm{dis,bio}}$ and $O_{2,\mathrm{soft}}$ distributions are shown.

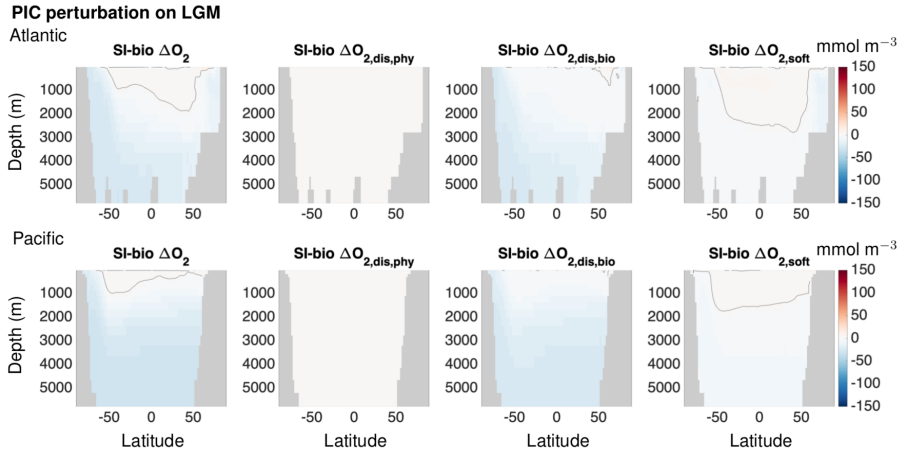

Figure A.19: Zonally-averaged O_2 components in the Atlantic basin (top row) and Pacific basin (bottom row) for the PIC sea ice light limitation perturbation experiment on the LGM. The O_2, $O_{2,\mathrm{dis,phy}}$, $O_{2,\mathrm{dis,bio}}$ and $O_{2,\mathrm{soft}}$ distributions are shown.

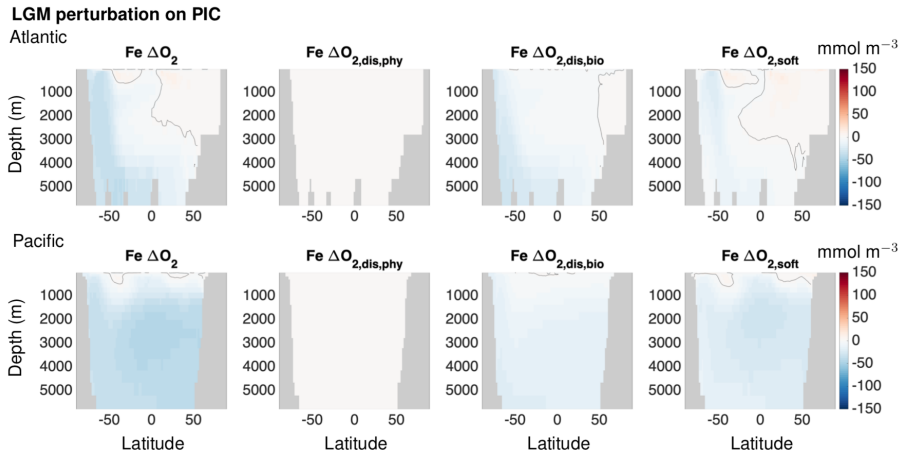

Figure A.20: Zonally-averaged O_2 components in the Atlantic basin (top row) and Pacific basin (bottom row) for the LGM iron fertilization perturbation experiment on the PIC. The O_2, $O_{2,\mathrm{dis,phy}}$, $O_{2,\mathrm{dis,bio}}$ and $O_{2,\mathrm{soft}}$ distributions are shown.

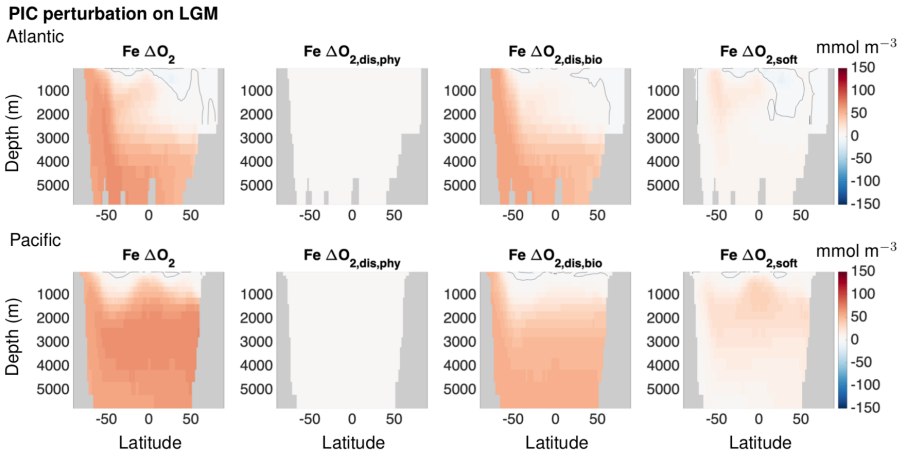

Figure A.21: Zonally-averaged O_2 components in the Atlantic basin (top row) and Pacific basin (bottom row) for the LGM iron fertilization perturbation experiment on the PIC. The O_2, $O_{2,\mathrm{dis,phy}}$, $O_{2,\mathrm{dis,bio}}$ and $O_{2,\mathrm{soft}}$ distributions are shown.

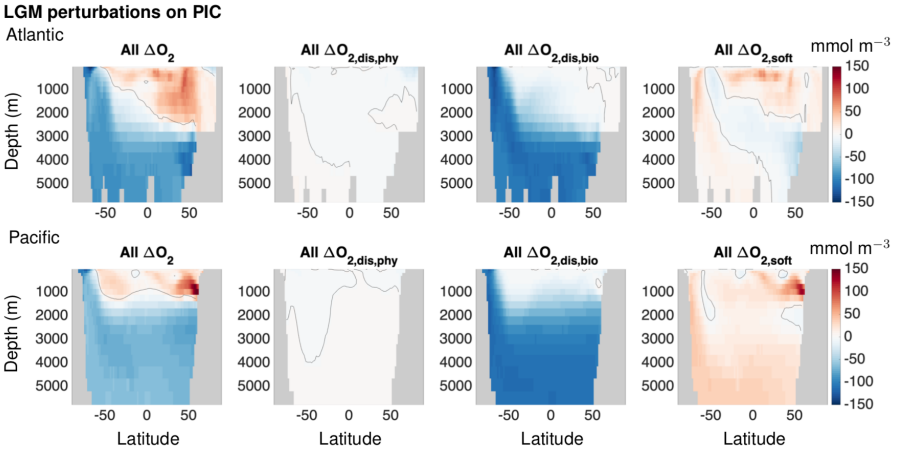

Figure A.22: Zonally-averaged O_2 components in the Atlantic basin (top row) and Pacific basin (bottom row) for the LGM "All" perturbation on PIC. The "All" perturbation includes temperature, circulation, sea ice, iron, and a 1 PSU salinity increase consistent with 110 m sea level drop in the LGM. The O_2, $O_{2,\mathrm{dis,phy}}$, $O_{2,\mathrm{dis,bio}}$ and $O_{2,\mathrm{soft}}$ distributions are shown.

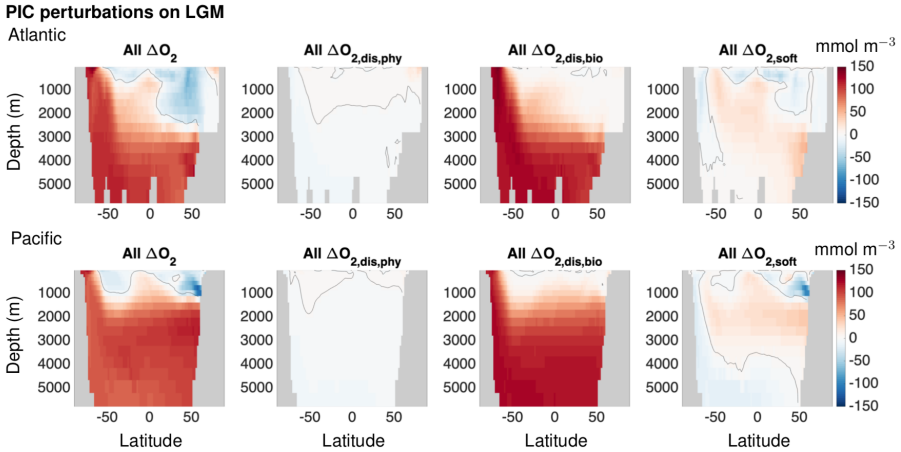

Figure A.23: Zonally-averaged O_2 components in the Atlantic basin (top row) and Pacific basin (bottom row) for the PIC "All" perturbation on LGM. The "All" perturbation includes temperature, circulation, sea ice, iron, and a 1 PSU salinity decrease consistent with 110 m sea level rise in the PIC. The O_2, $O_{2,\mathrm{dis,phy}}$, $O_{2,\mathrm{dis,bio}}$ and $O_{2,\mathrm{soft}}$ distributions are shown.

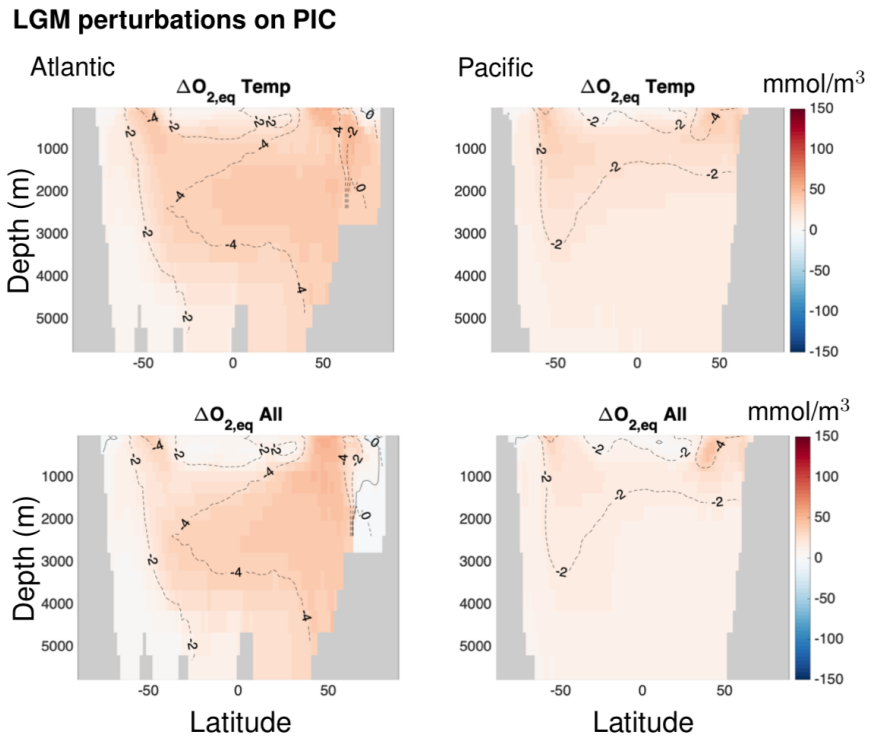

Figure A.24: Zonally-averaged $O_{2,eq}$ in the Atlantic (left) and Pacific (right) basins for LGM perturbations on PIC. Distribution of $O_{2,eq}$ is shown for the perturbation of LGM temperature (top) and "All" perturbations (bottom) on the PIC. Contours show the zonally-averaged temperature difference (°C) between the LGM and PIC.

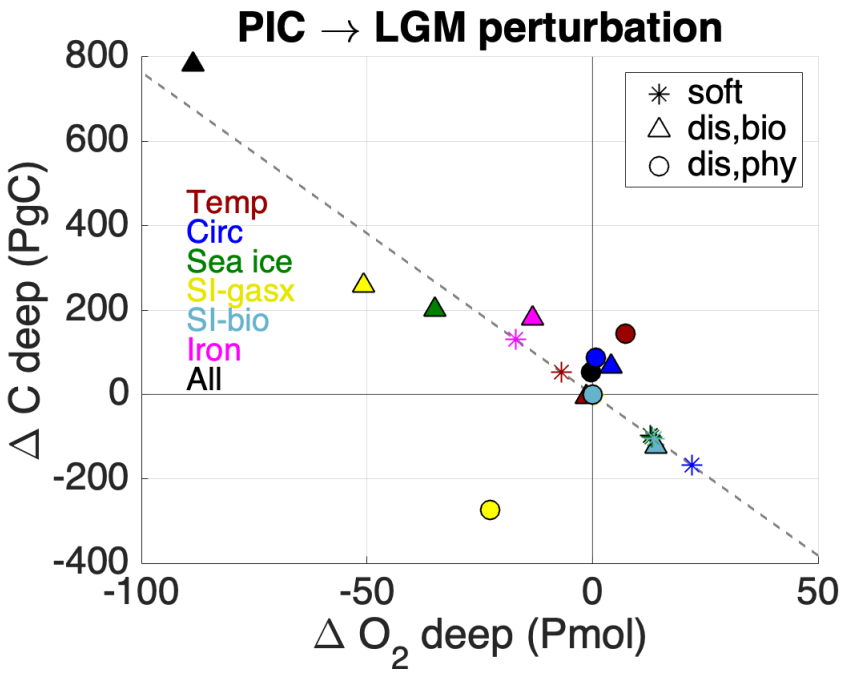

Figure A.25: The effect of LGM perturbations on the individual components of O_2 and DIC are shown. Soft tissue (asterisk), biological disequilibrium (triangle) and physical disequilibrium (circle) components are plotted. The perturbation experiments shown are temperature (dark red), circulation (dark blue), sea ice (green), sea ice gas-exchange (SI-gasx: yellow), sea ice light limitation on biology (SI-bio: light blue), iron fertilization (magenta) and the "All" perturbation (black). The sea ice physical disequilibrium point lies directly under the sea ice gas-exchange physical disequilibrium point. The dashed grey line represents the (negative of the) Redfield C:$-O_2$ ratio.

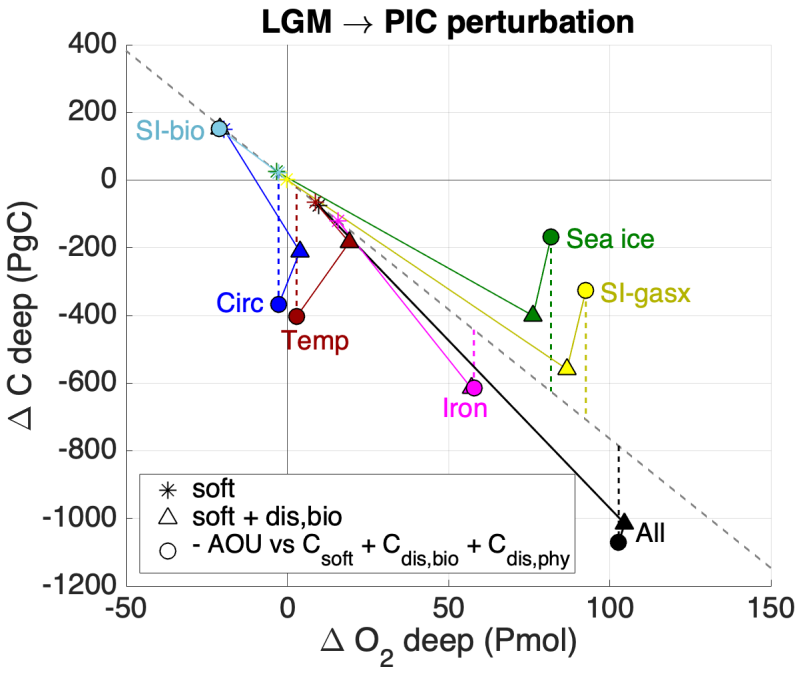

Figure A.26: Relationship between ΔO_2, ΔAOU and biological carbon storage in the LGM with PIC perturbations. ΔO_2 versus ΔC in the deep ocean (below 1000 m) for the perturbation experiments where a PIC condition is imposed on the LGM configuration. Changes are shown for the following perturbations: "All" (black); sea ice (green) which is further separated into the gas exchange effect (SI-gasx, yellow), and biological light limitation effect (SI-bio, light blue); iron fertilization (pink); temperature (red); and circulation (dark blue). For each perturbation three components of the carbon-oxygen system are shown: soft-tissue components ($\Delta O_{2,\mathrm{soft}}$ and ΔC_{soft}) (stars); soft-tissue and biological disequilibrium components ($\Delta O_{2,\mathrm{soft}} + \Delta O_{2,\mathrm{dis,bio}}$ and ΔC_{bio}) (triangles); total O_2 and C change from soft-tissue, biological and physical disequilibrium (ΔAOU and $\Delta C_{\mathrm{bio}} + \Delta C_{\mathrm{dis,phy}}$). The dashed grey line represents the (negative of the) Redfield C:$-O_2$ ratio.

Bibliography

[1] J. G. Canadell et al. “Chapter 5: Global Carbon and Other Biogeochemical Cycles and Feedbacks”. In: *Climate Change 2021: The Physical Science Basis. Contribution of Working Group I to the Sixth Assessment Report of the Intergovernmental Panel on Climate Change*. Ed. by V. Masson-Delmotte et al. Cambridge, United Kingom and New York, NY, USA: Cambridge University Press, 2021, pp. 673–816.

[2] R. E. Zeebe and D. Wolf-Gladrow. *CO2 in Seawater: Equilibrium, Kinetics, Isotopes*. Gulf Professional Publishing, Oct. 15, 2001. 382 pp. Google Books: g3j3Zn4kEscC.

[3] Tyler Volk and Martin I. Hoffert. “Ocean Carbon Pumps: Analysis of Relative Strengths and Efficiencies in Ocean-Driven Atmospheric CO2 Changes”. In: *The Carbon Cycle and Atmospheric CO2: Natural Variations Archean to Present*. American Geophysical Union (AGU), 1985, pp. 99–110. URL: https://onlinelibrary.wiley.com/doi/abs/10.1029/GM032p0099 (visited on 09/02/2022).

[4] Irina Marinov and Jorge L. Sarmiento. “The Role of the Oceans in the Global Carbon Cycle: An Overview”. In: *The Ocean Carbon Cycle and Climate*. Ed. by Mick Follows and Temel Oguz. Dordrecht: Springer Netherlands, 2004, pp. 251–295. URL: http://link.springer.com/10.1007/978-1-4020-2087-2_8 (visited on 04/20/2022).

[5] Laurence A. Anderson and Jorge L. Sarmiento. “Redfield Ratios of Remineralization Determined by Nutrient Data Analysis”. In: *Global Biogeochemical Cycles* 8.1 (1994), pp. 65–80. URL: https://onlinelibrary.wiley.com/doi/abs/10.1029/93GB03318 (visited on 08/10/2022).

[6] Samuel L. Jaccard and Eric D. Galbraith. “Large Climate-Driven Changes of Oceanic Oxygen Concentrations during the Last Deglaciation”. In: *Nature Geoscience* 5.2 (Feb. 2012), pp. 151–156. URL: http://www.nature.com/articles/ngeo1352 (visited on 09/10/2022).

[7] Robert F. Anderson et al. “Deep-Sea Oxygen Depletion and Ocean Carbon Sequestration During the Last Ice Age”. In: *Global Biogeochemical Cycles* 33.3 (Mar. 2019), pp. 301–317. URL: https://onlinelibrary.wiley.com/doi/abs/10.1029/2018GB006049 (visited on 02/14/2022).

[8] Daniel M. Sigman, Mathis P. Hain, and Gerald H. Haug. "The Polar Ocean and Glacial Cycles in Atmospheric CO2 Concentration". In: *Nature* 466.7302 (July 2010), pp. 47–55. URL: http://www.nature.com/articles/nature09149 (visited on 02/14/2022).

[9] Wallace S Broecker. "Glacial to Interglacial Changes in Ocean Chemistry". In: *Progress in Oceanography* 11 (1982), pp. 151–197.

[10] Britton B. Stephens and Ralph F. Keeling. "The Influence of Antarctic Sea Ice on Glacial–Interglacial CO2 Variations". In: *Nature* 404.6774 (6774 Mar. 2000), pp. 171–174. URL: https://www.nature.com/articles/35004556 (visited on 07/28/2022).

[11] David Ferreira et al. "Linking Glacial-Interglacial States to Multiple Equilibria of Climate". In: *Geophysical Research Letters* 45.17 (2018), pp. 9160–9170. URL: https://onlinelibrary.wiley.com/doi/abs/10.1029/2018GL077019 (visited on 09/09/2022).

[12] John H. Martin. "Glacial-Interglacial CO2 Change: The Iron Hypothesis". In: *Paleoceanography* 5.1 (1990), pp. 1–13. URL: https://onlinelibrary.wiley.com/doi/abs/10.1029/PA005i001p00001 (visited on 06/29/2022).

[13] Akitomo Yamamoto et al. "Glacial CO2 Decrease and Deep-Water Deoxygenation by Iron Fertilization from Glaciogenic Dust". In: *Climate of the Past* 15.3 (June 4, 2019), pp. 981–996. URL: https://cp.copernicus.org/articles/15/981/2019/ (visited on 02/14/2022).

[14] J. Yu et al. "Sequestration of Carbon in the Deep Atlantic during the Last Glaciation". In: *Nature Geoscience* 9.4 (Apr. 2016), pp. 319–324. URL: http://www.nature.com/articles/ngeo2657 (visited on 02/14/2022).

[15] L. C. Skinner et al. "Radiocarbon Constraints on the Glacial Ocean Circulation and Its Impact on Atmospheric CO2". In: *Nature Communications* 8.1 (Dec. 2017), p. 16010. URL: http://www.nature.com/articles/ncomms16010 (visited on 02/14/2022).

[16] Wallace S Broecker and Tsung-Hung Peng. "Carbon Cycle: 1985 Glacial to Interglacial Changes in the Operation of the Global Carbon Cycle". In: *Radiocarbon* 28 (2A 1986), pp. 309–327. URL: https://www.cambridge.org/core/product/identifier/S0033822200007414/type/journal_article (visited on 05/30/2022).

[17] David Archer et al. "What Caused the Glacial/Interglacial Atmospheric pCO2 Cycles?" In: *Reviews of Geophysics* 38.2 (May 2000), pp. 159–189. URL: http://doi.wiley.com/10.1029/1999RG000066 (visited on 02/14/2022).

[18] Daniel M. Sigman and Edward A. Boyle. "Glacial/Interglacial Variations in Atmospheric Carbon Dioxide". In: *Nature* 407.6806 (Oct. 2000), pp. 859–869. URL: http://www.nature.com/articles/35038000 (visited on 02/14/2022).

[19] Richard G. Williams and Michael J. Follows. *Ocean Dynamics and the Carbon Cycle: Principles and Mechanisms*. Cambridge University Press, July 14, 2011. 433 pp. Google Books: dfTJdgZg260C.

[20] S. Khatiwala, A. Schmittner, and J. Muglia. "Air-Sea Disequilibrium Enhances Ocean Carbon Storage during Glacial Periods". In: *Science Advances* 5.6 (June 7, 2019), eaaw4981. URL: https://www.science.org/doi/10.1126/sciadv.aaw4981 (visited on 02/14/2022).

[21] Eric D. Galbraith and Samuel L. Jaccard. "Deglacial Weakening of the Oceanic Soft Tissue Pump: Global Constraints from Sedimentary Nitrogen Isotopes and Oxygenation Proxies". In: *Quaternary Science Reviews* 109 (Feb. 2015), pp. 38–48. URL: https://linkinghub.elsevier.com/retrieve/pii/S0277379114004697 (visited on 02/14/2022).

[22] A. Schmittner and C. J. Somes. "Complementary Constraints from Carbon (^{13} C) and Nitrogen (^{15} N) Isotopes on the Glacial Ocean's Soft-tissue Biological Pump". In: *Paleoceanography* 31.6 (June 2016), pp. 669–693. URL: https://onlinelibrary.wiley.com/doi/abs/10.1002/2015PA002905 (visited on 02/14/2022).

[23] J. L. Sarmiento and N. Gruber. *Ocean Biogeochemical Dynamics*. 1st ed. Princeton NJ: Princeton University Press, 2006.

[24] J. L. Russell and A. G. Dickson. "Variability in Oxygen and Nutrients in South Pacific Antarctic Intermediate Water". In: *Global Biogeochemical Cycles* 17.2 (2003). URL: https://onlinelibrary.wiley.com/doi/abs/10.1029/2000GB001317 (visited on 08/04/2022).

[25] T. Ito, M. J. Follows, and E. A. Boyle. "Is AOU a Good Measure of Respiration in the Oceans?: AOU AND RESPIRATION". In: *Geophysical Research Letters* 31.17 (Sept. 2004), n/a–n/a. URL: http://doi.wiley.com/10.1029/2004GL020900 (visited on 02/14/2022).

[26] O. Duteil et al. "A Novel Estimate of Ocean Oxygen Utilisation Points to a Reduced Rate of Respiration in the Ocean Interior". In: *Biogeosciences* 10.11 (Nov. 28, 2013), pp. 7723–7738. URL: https://bg.copernicus.org/articles/10/7723/2013/ (visited on 02/14/2022).

[27] W. Koeve and P. Kähler. "Oxygen Utilization Rate (OUR) Underestimates Ocean Respiration: A Model Study: OUR Underestimates Ocean Respiration". In: *Global Biogeochemical Cycles* 30.8 (Aug. 2016), pp. 1166–1182. URL: http://doi.wiley.com/10.1002/2015GB005354 (visited on 02/14/2022).

[28] N. Anderson, ed. *The Fate of Fossil Fuel CO2 in the Oceans*. Springer New York NY, 1977. 749 pp. URL: https://link.springer.com/book/9781489950185 (visited on 06/29/2022).

[29] N.J. Shackleton. "Tropical Rainforest History and the Equatorial Pacific Carbonate Dissolution Cycle". In: *The Fate of Fossil Fuel CO2 in the Oceans*. Ed. by N. Anderson. 1st ed. New York, NY: Springer, 1977, p. 749.

[30] Robert J. Delmas, Jean-Marc Ascencio, and Michel Legrand. "Polar Ice Evidence That Atmospheric CO2 20,000 Yr BP Was 50% of Present". In: *Nature* 284.5752 (5752 Mar. 1980), pp. 155–157. URL: https://www.nature.com/articles/284155a0 (visited on 06/29/2022).

[31] Werner Berner, Hans Oeschger, and Bernhard Stauffer. "Information on the CO2 Cycle from Ice Core Studies". In: *Radiocarbon* 22.2 (1980/ed), pp. 227–235. URL: https://www.cambridge.org/core/journals/radiocarbon/article/information-on-the-co2-cycle-from-ice-core-studies/D137FFE323148623AB8A187F9EED1899 (visited on 06/29/2022).

[32] R. E. M. Rickaby and H. Elderfield. "Planktonic Foraminiferal Cd/Ca: Paleonutrients or Paleotemperature?" In: *Paleoceanography* 14.3 (June 1999), pp. 293–303. URL: http://doi.wiley.com/10.1029/1999PA900007 (visited on 09/09/2022).

[33] H. Elderfield and R. E. M. Rickaby. "Oceanic Cd/P Ratio and Nutrient Utilization in the Glacial Southern Ocean". In: *Nature* 405.6784 (6784 May 2000), pp. 305–310. URL: https://www.nature.com/articles/35012507 (visited on 09/02/2022).

[34] K. Wallmann, B. Schneider, and M. Sarnthein. "Effects of Eustatic Sea-Level Change, Ocean Dynamics, and Nutrient Utilization on Atmospheric pCO_2 and Seawater Composition over the Last 130 000 Years: A Model Study". In: *Climate of the Past* 12.2 (Feb. 18, 2016), pp. 339–375. URL: https://cp.copernicus.org/articles/12/339/2016/ (visited on 09/09/2022).

[35] C. M. Moore et al. "Processes and Patterns of Oceanic Nutrient Limitation". In: *Nature Geoscience* 6.9 (Sept. 2013), pp. 701–710. URL: http://www.nature.com/articles/ngeo1765 (visited on 09/09/2022).

[36] Wallace S. Broecker and Gideon M. Henderson. "The Sequence of Events Surrounding Termination II and Their Implications for the Cause of Glacial-Interglacial CO $_2$ Changes". In: *Paleoceanography* 13.4 (Aug. 1998), pp. 352–364. URL: http://doi.wiley.com/10.1029/98PA00920 (visited on 09/09/2022).

[37] Laurent Bopp et al. "Dust Impact on Marine Biota and Atmospheric CO $_2$ during Glacial Periods: LGM DUST, MARINE BIOTA, AND ATMOSPHERIC PCO $_2$". In: *Paleoceanography* 18.2 (June 2003), n/a–n/a. URL: http://doi.wiley.com/10.1029/2002PA000810 (visited on 02/14/2022).

[38] Elizabeth M. Shoenfelt et al. "Highly Bioavailable Dust-Borne Iron Delivered to the Southern Ocean during Glacial Periods". In: *Proceedings of the National Academy of Sciences* 115.44 (Oct. 30, 2018), pp. 11180–11185. URL: http://www.pnas.org/lookup/doi/10.1073/pnas.1809755115 (visited on 02/14/2022).

[39] Kazuhiro Misumi et al. "Humic Substances May Control Dissolved Iron Distributions in the Global Ocean: Implications from Numerical Simulations". In: *Global Biogeochemical Cycles* 27.2 (2013), pp. 450–462. URL: https://onlinelibrary.wiley.com/doi/abs/10.1002/gbc.20039 (visited on 09/09/2022).

[40] Alessandro Tagliabue et al. "How Well Do Global Ocean Biogeochemistry Models Simulate Dissolved Iron Distributions?: GLOBAL IRON MODELS". In: *Global Biogeochemical Cycles* 30.2 (Feb. 2016), pp. 149–174. URL: http://doi.wiley.com/10.1002/2015GB005289 (visited on 09/09/2022).

[41] Eric D. Galbraith and Luke C. Skinner. "The Biological Pump During the Last Glacial Maximum". In: *Annual Review of Marine Science* 12.1 (Jan. 3, 2020), pp. 559–586. URL: https://www.annualreviews.org/doi/10.1146/annurev-marine-010419-010906 (visited on 02/14/2022).

[42] Bradley N. Opdyke and James C.G. Walker. "Return of the Coral Reef Hypothesis: Basin to Shelf Partitioning of CaCO3 and Its Effect on Atmospheric CO2". In: *Geology* 20.8 (Aug. 1, 1992), pp. 733–736. URL: https://doi.org/10.1130/0091-7613(1992)020<0733:ROTCRH>2.3.CO;2 (visited on 09/09/2022).

[43] D. Archer and E. Maier-Reimer. "Effect of Deep-Sea Sedimentary Calcite Preservation on Atmospheric CO2 Concentration". In: *Nature* 367.6460 (6460 Jan. 1994), pp. 260–263. URL: https://www.nature.com/articles/367260a0 (visited on 09/09/2022).

[44] Daniel M. Sigman, Daniel C. McCorkle, and William R. Martin. "The Calcite Lysocline as a Constraint on Glacial/Interglacial Low-Latitude Production Changes". In: *Global Biogeochemical Cycles* 12.3 (1998), pp. 409–427. URL: https://onlinelibrary.wiley.com/doi/abs/10.1029/98GB01184 (visited on 09/09/2022).

[45] J. R. Toggweiler. "Variation of Atmospheric CO $_2$ by Ventilation of the Ocean's Deepest Water". In: *Paleoceanography* 14.5 (Oct. 1999), pp. 571–588. URL: http://doi.wiley.com/10.1029/1999PA900033 (visited on 09/09/2022).

[46] *Home | PMIP*. URL: https://pmip.lsce.ipsl.fr/ (visited on 09/02/2022).

[47] C. Waelbroeck et al. "Constraints on the Magnitude and Patterns of Ocean Cooling at the Last Glacial Maximum". In: *Nature Geoscience* 2.2 (2 Feb. 2009), pp. 127–132. URL: https://www.nature.com/articles/ngeo411 (visited on 09/09/2022).

[48] Verena Benz et al. "Last Glacial Maximum Sea Surface Temperature and Sea-Ice Extent in the Pacific Sector of the Southern Ocean". In: *Quaternary Science Reviews* 146 (Aug. 15, 2016), pp. 216–237. URL: https://www.sciencedirect.com/science/article/pii/S0277379116302062 (visited on 09/09/2022).

[49] T.M. Conway et al. "Constraints on Soluble Aerosol Iron Flux to the Southern Ocean at the Last Glacial Maximum". In: *Nature Communications* 6.1 (Nov. 2015), p. 7850. URL: http://www.nature.com/articles/ncomms8850 (visited on 09/09/2022).

[50] Hugh C. Jenkyns. "Geochemistry of Oceanic Anoxic Events". In: *Geochemistry, Geophysics, Geosystems* 11.3 (2010). URL: https://onlinelibrary.wiley.com/doi/abs/10.1029/2009GC002788 (visited on 09/02/2022).

[51] Sunke Schmidtko, Lothar Stramma, and Martin Visbeck. "Decline in Global Oceanic Oxygen Content during the Past Five Decades". In: *Nature* 542.7641 (Feb. 2017), pp. 335–339. URL: http://www.nature.com/articles/nature21399 (visited on 02/14/2022).

[52] G. P Klinkhammer and M. R Palmer. "Uranium in the Oceans: Where It Goes and Why". In: *Geochimica et Cosmochimica Acta* 55.7 (July 1, 1991), pp. 1799–1806. URL: https://www.sciencedirect.com/science/article/pii/001670379190024Y (visited on 08/20/2022).

[53] Roger François et al. "Contribution of Southern Ocean Surface-Water Stratification to Low Atmospheric CO2 Concentrations during the Last Glacial Period". In: *Nature* 389.6654 (Oct. 1997), pp. 929–935. URL: http://www.nature.com/articles/40073 (visited on 02/14/2022).

[54] Kassandra M. Costa et al. "Trace Element (Mn, Zn, Ni, V) and Authigenic Uranium (aU) Geochemistry Reveal Sedimentary Redox History on the Juan de Fuca Ridge, North Pacific Ocean". In: *Geochimica et Cosmochimica Acta*. Chemistry of Oceans Past and Present: A Special Issue in Tribute to Harry Elderfield 236 (Sept. 1, 2018), pp. 79–98. URL: https://www.sciencedirect.com/science/article/pii/S0016703718300863 (visited on 08/20/2022).

[55] William W. Bennett and Donald E. Canfield. "Redox-Sensitive Trace Metals as Paleoredox Proxies: A Review and Analysis of Data from Modern Sediments". In: *Earth-Science Reviews* 204 (May 2020), p. 103175. URL: https://linkinghub.elsevier.com/retrieve/pii/S001282522030221X (visited on 09/02/2022).

[56] Wanyi Lu et al. "Comparing Paleo-Oxygenation Proxies (Benthic Foraminiferal Surface Porosity, I/Ca, Authigenic Uranium) on Modern Sediments and the Glacial Arabian Sea". In: *Geochimica et Cosmochimica Acta* 331 (Aug. 2022), pp. 69–85. URL: https://linkinghub.elsevier.com/retrieve/pii/S0016703722002666 (visited on 01/05/2023).

[57] L.I. Bradtmiller et al. "A Deeper Respired Carbon Pool in the Glacial Equatorial Pacific Ocean". In: *Earth and Planetary Science Letters* 299.3-4 (Nov. 2010), pp. 417–425. URL: https://linkinghub.elsevier.com/retrieve/pii/S0012821X10005972 (visited on 02/14/2022).

[58] A.W. Jacobel et al. "Deep Pacific Storage of Respired Carbon during the Last Ice Age: Perspectives from Bottom Water Oxygen Reconstructions". In: *Quaternary Science Reviews* 230 (Feb. 2020), p. 106065. URL: https://linkinghub.elsevier.com/retrieve/pii/S0277379119306456 (visited on 02/14/2022).

[59] Axel Durand et al. "Reduced Oxygenation at Intermediate Depths of the Southwest Pacific during the Last Glacial Maximum". In: *Earth and Planetary Science Letters* 491 (June 1, 2018), pp. 48–57. URL: https://www.sciencedirect.com/science/article/pii/S0012821X18301602 (visited on 09/09/2022).

[60] Wanyi Lu et al. "I/Ca in Epifaunal Benthic Foraminifera: A Semi-Quantitative Proxy for Bottom Water Oxygen in a Multi-Proxy Compilation for Glacial Ocean Deoxygenation". In: *Earth and Planetary Science Letters* 533 (Mar. 2020), p. 116055. URL: https://linkinghub.elsevier.com/retrieve/pii/S0012821X19307514 (visited on 02/14/2022).

[61] Babette A. A. Hoogakker et al. "Glacial Expansion of Oxygen-Depleted Seawater in the Eastern Tropical Pacific". In: *Nature* 562.7727 (7727 Oct. 2018), pp. 410–413. URL: https://www.nature.com/articles/s41586-018-0589-x (visited on 09/09/2022).

[62] N. Glock, V. Liebetrau, and A. Eisenhauer. "I/Ca Ratios in Benthic Foraminifera from the Peruvian Oxygen Minimum Zone: Analytical Methodology and Evaluation as a Proxy for Redox Conditions". In: *Biogeosciences* 11.23 (Dec. 12, 2014), pp. 7077–7095. URL: https://bg.copernicus.org/articles/11/7077/2014/bg-11-7077-2014-discussion.html (visited on 09/02/2022).

[63] Zunli Lu et al. "Oxygen Depletion Recorded in Upper Waters of the Glacial Southern Ocean". In: *Nature Communications* 7 (Mar. 31, 2016), p. 11146. pmid: 27029225.

[64] Daniel C McCorkle and Steven R Emerson. "The Relationship between Pore Water Carbon Isotopic Composition and Bottom Water Oxygen Concentration". In: *Geochimica et Cosmochimica Acta* 52.5 (May 1, 1988), pp. 1169–1178. URL: https://www.sciencedirect.com/science/article/pii/0016703788902700 (visited on 09/09/2022).

[65] Babette A. A. Hoogakker et al. "Glacial–Interglacial Changes in Bottom-Water Oxygen Content on the Portuguese Margin". In: *Nature Geoscience* 8.1 (Jan. 2015), pp. 40–43. URL: http://www.nature.com/articles/ngeo2317 (visited on 02/14/2022).

[66] Julia Gottschalk et al. "Biological and Physical Controls in the Southern Ocean on Past Millennial-Scale Atmospheric CO2 Changes". In: *Nature Communications* 7.1 (Sept. 2016), p. 11539. URL: http://www.nature.com/articles/ncomms11539 (visited on 02/14/2022).

[67] Daniel C. McCorkle et al. "The Influence of Microhabitats on the Carbon Isotopic Composition of Deep-Sea Benthic Foraminifera". In: *Paleoceanography* 5.2 (1990), pp. 161–185. URL: https://onlinelibrary.wiley.com/doi/abs/10.1029/PA005i002p00161 (visited on 09/09/2022).

[68] Anthony E. Rathburn et al. "A New Biological Proxy for Deep-Sea Paleo-Oxygen: Pores of Epifaunal Benthic Foraminifera". In: *Scientific Reports* 8.1 (Dec. 2018), p. 9456. URL: http://www.nature.com/articles/s41598-018-27793-4 (visited on 09/09/2022).

[69] S.L. Jaccard et al. "Subarctic Pacific Evidence for a Glacial Deepening of the Oceanic Respired Carbon Pool". In: *Earth and Planetary Science Letters* 277.1-2 (Jan. 2009), pp. 156–165. URL: https://linkinghub.elsevier.com/retrieve/pii/S0012821X08006754 (visited on 09/02/2022).

[70] Taro Takahashi, Wallace S. Broecker, and Sara Langer. "Redfield Ratio Based on Chemical Data from Isopycnal Surfaces". In: *Journal of Geophysical Research: Oceans* 90.C4 (1985), pp. 6907–6924. URL: https://onlinelibrary.wiley.com/doi/abs/10.1029/JC090iC04p06907 (visited on 08/10/2022).

[71] Tim DeVries and Curtis Deutsch. "Large-Scale Variations in the Stoichiometry of Marine Organic Matter Respiration". In: *Nature Geoscience* 7.12 (Dec. 2014), pp. 890–894. URL: http://www.nature.com/articles/ngeo2300 (visited on 05/30/2022).

[72] Tatsuro Tanioka, Katsumi Matsumoto, and Michael W. Lomas. "Drawdown of Atmospheric pCO2 Via Variable Particle Flux Stoichiometry in the Ocean Twilight Zone". In: *Geophysical Research Letters* 48.22 (2021), e2021GL094924. URL: https://onlinelibrary.wiley.com/doi/abs/10.1029/2021GL094924 (visited on 02/09/2022).

[73] Malin Ödalen et al. "Variable CP Composition of Organic Production and Its Effect on Ocean Carbon Storage in Glacial-like Model Simulations". In: *Biogeosciences* 17.8 (Apr. 22, 2020), pp. 2219–2244. URL: https://bg.copernicus.org/articles/17/2219/2020/ (visited on 02/14/2022).

[74] Andreas Oschlies et al. "Drivers and Mechanisms of Ocean Deoxygenation". In: *Nature Geoscience* 11.7 (July 2018), pp. 467–473. URL: http://www.nature.com/articles/s41561-018-0152-2 (visited on 02/09/2022).

[75] A. L. Gordon, C. T. A. Chen, and W. G. Metcalf. "Winter Mixed Layer Entrainment of Weddell Deep Water". In: *Journal of Geophysical Research: Oceans* 89.C1 (1984), pp. 637–640. URL: https://onlinelibrary.wiley.com/doi/abs/10.1029/JC089iC01p00637 (visited on 08/04/2022).

[76] Mitchell K. Wolf et al. "Oxygen Saturation Surrounding Deep Water Formation Events in the Labrador Sea From Argo-O $_2$ Data". In: *Global Biogeochemical Cycles* 32.4 (Apr. 2018), pp. 635–653. URL: https://onlinelibrary.wiley.com/doi/10.1002/2017GB005829 (visited on 02/14/2022).

[77] Takamitsu Ito and Michael J. Follows. "Air-Sea Disequilibrium of Carbon Dioxide Enhances the Biological Carbon Sequestration in the Southern Ocean: DISEQUILIBRIUM CARBON PUMP". In: *Global Biogeochemical Cycles* 27.4 (Dec. 2013), pp. 1129–1138. URL: http://doi.wiley.com/10.1002/2013GB004682 (visited on 02/14/2022).

[78] Rik Wanninkhof. "Relationship between Wind Speed and Gas Exchange over the Ocean". In: *Journal of Geophysical Research* 97.C5 (1992), p. 7373. URL: http://doi.wiley.com/10.1029/92JC00188 (visited on 02/14/2022).

[79] Sarah Eggleston and Eric D. Galbraith. "The Devil's in the Disequilibrium: Multi-Component Analysis of Dissolved Carbon and Oxygen Changes under a Broad Range of Forcings in a General Circulation Model". In: *Biogeosciences* 15.12 (June 20, 2018), pp. 3761–3777. URL: https://bg.copernicus.org/articles/15/3761/2018/ (visited on 02/14/2022).

[80] Juan Muglia, Luke C. Skinner, and Andreas Schmittner. "Weak Overturning Circulation and High Southern Ocean Nutrient Utilization Maximized Glacial Ocean Carbon". In: *Earth and Planetary Science Letters* 496 (Aug. 2018), pp. 47–56. URL: https://linkinghub.elsevier.com/retrieve/pii/S0012821X18303212 (visited on 02/14/2022).

[81] Katsumi Matsumoto, Taketo Hashioka, and Yasuhiro Yamanaka. "Effect of Temperature-Dependent Organic Carbon Decay on Atmospheric pCO2". In: *Journal of Geophysical Research: Biogeosciences* 112.G2 (2007). URL: https://onlinelibrary.wiley.com/doi/abs/10.1029/2006JG000187 (visited on 09/09/2022).

[82] M. Sarnthein, B. Schneider, and P. M. Grootes. "Peak Glacial ^{14}C Ventilation Ages Suggest Major Draw-down of Carbon into the Abyssal Ocean". In: *Climate of the Past* 9.6 (Nov. 15, 2013), pp. 2595–2614. URL: https://cp.copernicus.org/articles/9/2595/2013/ (visited on 09/09/2022).

[83] Christopher J. Somes et al. "A Three-Dimensional Model of the Marine Nitrogen Cycle during the Last Glacial Maximum Constrained by Sedimentary Isotopes". In: *Frontiers in Marine Science* 4 (May 9, 2017), p. 108. URL: http://journal.frontiersin.org/article/10.3389/fmars.2017.00108/full (visited on 02/14/2022).

[84] Jean Lynch-Stieglitz. "The Atlantic Meridional Overturning Circulation and Abrupt Climate Change". In: *Annual Review of Marine Science* 9.1 (Jan. 3, 2017), pp. 83–104. URL: https://www.annualreviews.org/doi/10.1146/annurev-marine-010816-060415 (visited on 08/30/2022).

[85] Louisa I. Bradtmiller, Jerry F. McManus, and Laura F. Robinson. "231Pa/230Th Evidence for a Weakened but Persistent Atlantic Meridional Overturning Circulation during Heinrich Stadial 1". In: *Nature Communications* 5.1 (1 Dec. 18, 2014), p. 5817. URL: https://www.nature.com/articles/ncomms6817 (visited on 09/02/2022).

[86] Jörg Lippold et al. "Strength and Geometry of the Glacial Atlantic Meridional Overturning Circulation". In: *Nature Geoscience* 5.11 (Nov. 2012), pp. 813–816. URL: http://www.nature.com/articles/ngeo1608 (visited on 08/30/2022).

[87] Helena K. Evans and Ian R. Hall. "Deepwater Circulation on Blake Outer Ridge (Western North Atlantic) during the Holocene, Younger Dryas, and Last Glacial Maximum". In: *Geochemistry, Geophysics, Geosystems* 9.3 (2008). URL: https://onlinelibrary.wiley.com/doi/abs/10.1029/2007GC001771 (visited on 09/02/2022).

[88] Fabrice Lambert et al. “Dust Fluxes and Iron Fertilization in Holocene and Last Glacial Maximum Climates: DUST AND IRON FERTILIZATION”. In: *Geophysical Research Letters* 42.14 (July 28, 2015), pp. 6014–6023. URL: http://doi.wiley.com/10.1002/2015GL064250 (visited on 02/14/2022).

[89] Juan Muglia et al. “Combined Effects of Atmospheric and Seafloor Iron Fluxes to the Glacial Ocean: LAST GLACIAL MAXIMUM OCEAN IRON CYCLE”. In: *Paleoceanography* 32.11 (Nov. 2017), pp. 1204–1218. URL: http://doi.wiley.com/10.1002/2016PA003077 (visited on 02/14/2022).

[90] Samar Khatiwala, Martin Visbeck, and Mark A. Cane. “Accelerated Simulation of Passive Tracers in Ocean Circulation Models”. In: *Ocean Modelling* 9.1 (Jan. 2005), pp. 51–69. URL: https://linkinghub.elsevier.com/retrieve/pii/S1463500304000307 (visited on 09/07/2022).

[91] Samar Khatiwala. “A Computational Framework for Simulation of Biogeochemical Tracers in the Ocean: EFFICIENT OCEAN BIOGEOCHEMICAL MODELING”. In: *Global Biogeochemical Cycles* 21.3 (Sept. 2007), n/a–n/a. URL: http://doi.wiley.com/10.1029/2007GB002923 (visited on 09/07/2022).

[92] Ellen Cliff, Samar Khatiwala, and Andreas Schmittner. “Glacial Deep Ocean Deoxygenation Driven by Biologically Mediated Air–Sea Disequilibrium”. In: *Nature Geoscience* 14.1 (1 Jan. 2021), pp. 43–50. URL: https://www.nature.com/articles/s41561-020-00667-z (visited on 08/04/2022).

[93] Samuel L. Jaccard et al. “Covariation of Deep Southern Ocean Oxygenation and Atmospheric CO2 through the Last Ice Age”. In: *Nature* 530.7589 (Feb. 11, 2016), pp. 207–210. pmid: 26840491.

[94] S. Khatiwala, F. Primeau, and M. Holzer. “Ventilation of the Deep Ocean Constrained with Tracer Observations and Implications for Radiocarbon Estimates of Ideal Mean Age”. In: *Earth and Planetary Science Letters* 325–326 (Apr. 2012), pp. 116–125. URL: https://linkinghub.elsevier.com/retrieve/pii/S0012821X12000672 (visited on 02/14/2022).

[95] Andrew J. Weaver et al. “The UVic Earth System Climate Model: Model Description, Climatology, and Applications to Past, Present and Future Climates”. In: *Atmosphere-Ocean* 39.4 (Dec. 1, 2001), pp. 361–428. URL: https://www.tandfonline.com/doi/full/10.1080/07055900.2001.9649686 (visited on 09/09/2022).

[96] Samar Khatiwala. *Samarkhatiwala/Tmm: Version 2.0 of the Transport Matrix Method Software*. Zenodo, May 13, 2018. URL: https://zenodo.org/record/1246300 (visited on 09/10/2022).

[97] He Garcia et al. “World Ocean Atlas 2018, Volume 3: Dissolved Oxygen, Apparent Oxygen Utilization, and Dissolved Oxygen Saturation.” In: (Jan. 1, 2019). URL: https://archimer.ifremer.fr/doc/00651/76337/ (visited on 09/10/2022).

[98] Robert Drucker and Stephen C. Riser. "In Situ Phase-Domain Calibration of Oxygen Optodes on Profiling Floats". In: *Methods in Oceanography* 17 (Dec. 2016), pp. 296–318. URL: https://linkinghub.elsevier.com/retrieve/pii/S2211122016300019 (visited on 09/10/2022).

[99] Kenneth S. Johnson et al. *SOCCOM Float Data - Snapshot 2017-06-06*. Southern Ocean Carbon and Climate Observations and Modeling (SOCCOM) Float Data Archive. 2017. URL: http://library.ucsd.edu/dc/object/bb4985739g (visited on 09/10/2022).

[100] L. Bopp et al. "Multiple Stressors of Ocean Ecosystems in the 21st Century: Projections with CMIP5 Models". In: *Biogeosciences* 10.10 (Oct. 2, 2013), pp. 6225–6245. URL: https://bg.copernicus.org/articles/10/6225/2013/ (visited on 09/10/2022).

[101] Dorothea Bunzel et al. "A Multi-Proxy Analysis of Late Quaternary Ocean and Climate Variability for the Maldives, Inner Sea". In: *Climate of the Past* 13.12 (Dec. 13, 2017), pp. 1791–1813. URL: https://cp.copernicus.org/articles/13/1791/2017/ (visited on 02/14/2022).

[102] Natalie E. Umling and Robert C. Thunell. "Mid-Depth Respired Carbon Storage and Oxygenation of the Eastern Equatorial Pacific over the Last 25,000 Years". In: *Quaternary Science Reviews* 189 (June 2018), pp. 43–56. URL: https://linkinghub.elsevier.com/retrieve/pii/S0277379117307394 (visited on 02/14/2022).

[103] Karen E. Kohfeld et al. "Role of Marine Biology in Glacial-Interglacial CO $_2$ Cycles". In: *Science* 308.5718 (Apr. 2005), pp. 74–78. URL: https://www.science.org/doi/10.1126/science.1105375 (visited on 02/14/2022).

[104] Julia Gottschalk et al. "Carbon Isotope Offsets between Benthic Foraminifer Species of the Genus *Cibicides* (*Cibicidoides*) in the Glacial Sub-Antarctic Atlantic: EPIBENTHIC STABLE CARBON ISOTOPE OFFSETS". In: *Paleoceanography* 31.12 (Dec. 2016), pp. 1583–1602. URL: http://doi.wiley.com/10.1002/2016PA003029 (visited on 02/14/2022).

[105] Akira Oka et al. "Mechanisms Controlling Export Production at the LGM: Effects of Changes in Oceanic Physical Fields and Atmospheric Dust Deposition: SIMULATION OF EXPORT PRODUCTION AT LGM". In: *Global Biogeochemical Cycles* 25.2 (June 2011), n/a–n/a. URL: http://doi.wiley.com/10.1029/2009GB003628 (visited on 02/14/2022).

[106] Andreas Schmittner et al. "Large Fluctuations of Dissolved Oxygen in the Indian and Pacific Oceans during Dansgaard-Oeschger Oscillations Caused by Variations of North Atlantic Deep Water Subduction: OXYGEN DURING D/O OSCILLATIONS". In: *Paleoceanography* 22.3 (Sept. 2007), n/a–n/a. URL: http://doi.wiley.com/10.1029/2006PA001384 (visited on 02/14/2022).

[107] D.M. Roche, X. Crosta, and H. Renssen. "Evaluating Southern Ocean Sea-Ice for the Last Glacial Maximum and Pre-Industrial Climates: PMIP-2 Models and Data Evidence". In: *Quaternary Science Reviews* 56 (Nov. 2012), pp. 99–106. URL: https://linkinghub.elsevier.com/retrieve/pii/S027737911200371X (visited on 09/10/2022).

[108] James A. Smith et al. "The Presence of Polynyas in the Weddell Sea during the Last Glacial Period with Implications for the Reconstruction of Sea-Ice Limits and Ice Sheet History". In: *Earth and Planetary Science Letters* 296.3-4 (Aug. 2010), pp. 287–298. URL: https://linkinghub.elsevier.com/retrieve/pii/S0012821X10003262 (visited on 02/14/2022).

[109] Hannah Zanowski, Robert Hallberg, and Jorge L. Sarmiento. "Abyssal Ocean Warming and Salinification after Weddell Polynyas in the GFDL CM2G Coupled Climate Model". In: *Journal of Physical Oceanography* 45.11 (Nov. 2015), pp. 2755–2772. URL: https://journals.ametsoc.org/view/journals/phoc/45/11/jpo-d-15-0109.1.xml (visited on 09/10/2022).

[110] Eric D. Galbraith and Adam C. Martiny. "A Simple Nutrient-Dependence Mechanism for Predicting the Stoichiometry of Marine Ecosystems". In: *Proceedings of the National Academy of Sciences* 112.27 (July 7, 2015), pp. 8199–8204. URL: http://www.pnas.org/lookup/doi/10.1073/pnas.1423917112 (visited on 02/14/2022).

[111] Katsumi Matsumoto, Rosalind Rickaby, and Tatsuro Tanioka. "Carbon Export Buffering and CO2 Drawdown by Flexible Phytoplankton C:N:P Under Glacial Conditions". In: *Paleoceanography and Paleoclimatology* 35.7 (July 2020). URL: https://onlinelibrary.wiley.com/doi/10.1029/2019PA003823 (visited on 02/14/2022).

[112] Natalie M. Mahowald et al. "Atmospheric Iron Deposition: Global Distribution, Variability, and Human Perturbations". In: *Annual Review of Marine Science* 1.1 (2009), pp. 245–278. pmid: 21141037. URL: https://doi.org/10.1146/annurev.marine.010908.163727 (visited on 09/10/2022).

[113] Kurt Lambeck et al. "Sea Level and Global Ice Volumes from the Last Glacial Maximum to the Holocene". In: *Proceedings of the National Academy of Sciences* 111.43 (Oct. 28, 2014), pp. 15296–15303. URL: https://www.pnas.org/doi/10.1073/pnas.1411762111 (visited on 09/10/2022).

[114] Juan Muglia and Andreas Schmittner. "Glacial Atlantic Overturning Increased by Wind Stress in Climate Models". In: *Geophysical Research Letters* 42.22 (2015), pp. 9862–9868. URL: https://onlinelibrary.wiley.com/doi/abs/10.1002/2015GL064583 (visited on 09/10/2022).

[115] A. Abe-Ouchi et al. "Ice-Sheet Configuration in the CMIP5/PMIP3 Last Glacial Maximum Experiments". In: *Geoscientific Model Development* 8.11 (Nov. 6, 2015), pp. 3621–3637. URL: https://gmd.copernicus.org/articles/8/3621/2015/ (visited on 09/10/2022).

[116] Bernhard Bereiter et al. "Mean Global Ocean Temperatures during the Last Glacial Transition". In: *Nature* 553.7686 (Jan. 3, 2018), pp. 39–44. pmid: 29300008.

[117] Stuart D. Smith, Robin D. Muench, and Carol H. Pease. "Polynyas and Leads: An Overview of Physical Processes and Environment". In: *Journal of Geophysical Research* 95.C6 (1990), p. 9461. URL: http://doi.wiley.com/10.1029/JC095iC06p09461 (visited on 02/14/2022).

[118] Achim Stössel and Joong-Tae Kim. "Enhancing the Resolution of Sea Ice in a Global Ocean GCM". In: *Ocean Modelling* 11.1 (Jan. 1, 2006), pp. 28–48. URL: https://www.sciencedirect.com/science/article/pii/S1463500304000988 (visited on 09/09/2022).

[119] Xingren Wu, W. F. Budd, and Ian Allison. "Modelling the Impacts of Persistent Antarctic Polynyas with an Atmosphere–Sea-Ice General Circulation Model". In: *Deep Sea Research Part II: Topical Studies in Oceanography*. Recent Investigations of the Mertz Polynya and George Vth Land Continental Margin, East Antarctica 50.8 (May 1, 2003), pp. 1357–1372. URL: https://www.sciencedirect.com/science/article/pii/S0967064503000729 (visited on 09/09/2022).

[120] Xingchen Tony Wang et al. "Deep-Sea Coral Evidence for Lower Southern Ocean Surface Nitrate Concentrations during the Last Ice Age". In: *Proceedings of the National Academy of Sciences* 114.13 (Mar. 28, 2017), pp. 3352–3357. URL: https://www.pnas.org/doi/10.1073/pnas.1615718114 (visited on 09/10/2022).

[121] Samuel L. Jaccard and Eric D. Galbraith. "Large Climate-Driven Changes of Oceanic Oxygen Concentrations during the Last Deglaciation". In: *Nature Geoscience* 5.2 (Feb. 2012), pp. 151–156. URL: http://www.nature.com/articles/ngeo1352 (visited on 02/14/2022).